

### CERTIFICATION

We, the undersigned, declare that this report provides an accurate evaluation of data obtained from this study.

Kinetic Evaluation by: \_\_\_\_\_



Yuching Yang, Ph.D.  
Postdoctoral Fellow  
Center for Human Health Assessment  
The Hamner Institutes for Health Sciences

30-Mar-2010

Date

Reviewed and Approved by: \_\_\_\_\_



Harvey J. Clewell, III, Ph.D., DABT  
Director  
Center for Human Health Assessment  
The Hamner Institutes for Health Sciences

30-Mar-2010

Date

Reviewed and Approved by: \_\_\_\_\_

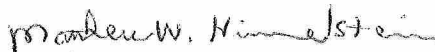


Steven R. Frame, D.V.M., Ph.D., Diplomate ACVP  
Manager  
DuPont Haskell

31-Mar-2010

Date

Issued by Study Director: \_\_\_\_\_



Matthew W. Himmelstein, Ph.D.  
Senior Research Toxicologist  
DuPont Haskell

31-Mar-2010

Date

## TABLE OF CONTENTS

	Page
<b>CERTIFICATION .....</b>	<b>2</b>
<b>TABLE OF CONTENTS .....</b>	<b>3</b>
<b>LIST OF TABLES .....</b>	<b>4</b>
<b>LIST OF FIGURES .....</b>	<b>4</b>
<b>LIST OF APPENDICES .....</b>	<b>6</b>
<b>STUDY INFORMATION .....</b>	<b>7</b>
<b>SUMMARY .....</b>	<b>8</b>
<b>INTRODUCTION.....</b>	<b>9</b>
<b>STUDY DESIGN.....</b>	<b>9</b>
<b>MATERIALS AND METHODS .....</b>	<b>9</b>
A. Test Substance .....	9
B. Test System.....	10
C. Microsome Preparation .....	10
D. Gas Chromatography Analysis .....	10
E. Microsomal Incubations.....	11
F. In Vitro Kinetic Model Description.....	12
G. Kinetic Parameter Point Estimation.....	12
H. Kinetic Parameter Probability (Bayesian) Analysis .....	12
<b>RESULTS AND DISCUSSION .....</b>	<b>15</b>
<b>CONCLUSIONS .....</b>	<b>16</b>
<b>RECORDS AND SAMPLE STORAGE .....</b>	<b>17</b>
<b>REFERENCES.....</b>	<b>17</b>
<b>TABLES.....</b>	<b>19</b>
<b>FIGURES.....</b>	<b>24</b>
<b>APPENDICES .....</b>	<b>63</b>

## LIST OF TABLES

	Page
Table 1	Stock microsomal protein concentrations and screen for total P450 protein ..... 20
Table 2	In vitro chloroprene metabolism prior distributions ..... 20
Table 3	Point estimate values for the microsomal oxidation of chloroprene without correction for background loss ..... 21
Table 4	Point estimate values for the microsomal oxidation of chloroprene with correction for background loss ..... 22
Table 5	Probability analysis of microsomal oxidation parameters for chloroprene ..... 23

## LIST OF FIGURES

	Page
Figure 1	Representative gas chromatography headspace calibration curve ..... 26
Figure 2	Chloroprene oxidative metabolism time course in male B6C3F1 mouse liver microsomes using point estimate model parameters ..... 27
Figure 3	Chloroprene oxidative metabolism time course in male B6C3F1 mouse lung microsomes using point estimate model parameters ..... 28
Figure 4	Chloroprene oxidative metabolism time course in male B6C3F1 mouse kidney microsomes using point estimate model parameters ..... 29
Figure 5	Chloroprene oxidative metabolism time course in female B6C3F1 mouse liver microsomes using point estimate model parameters ..... 30
Figure 6	Chloroprene oxidative metabolism time course in female B6C3F1 mouse lung microsomes using point estimate model parameters ..... 31
Figure 7	Chloroprene oxidative metabolism time course in female B6C3F1 mouse kidney microsomes using point estimate model parameters ..... 32
Figure 8	Chloroprene oxidative metabolism time course in male Fischer rat liver microsomes using point estimate model parameters ..... 33
Figure 9	Chloroprene oxidative metabolism time course in male Fischer rat lung microsomes using point estimate model parameters ..... 34
Figure 10	Chloroprene oxidative metabolism time course in male Fischer rat kidney microsomes using point estimate model parameters ..... 35
Figure 11	Chloroprene oxidative metabolism time course in female Fischer rat liver microsomes using point estimate model parameters ..... 36
Figure 12	Chloroprene oxidative metabolism time course in female Fischer rat lung microsomes using point estimate model parameters ..... 37
Figure 13	Chloroprene oxidative metabolism time course in female Fischer rat kidney microsomes using point estimate model parameters ..... 38

Figure 14	Chloroprene oxidative metabolism time course in human (pooled mixed gender) liver microsomes using point estimate model parameters.....	39
Figure 15	Chloroprene oxidative metabolism time course in human (pooled mixed gender) lung microsomes using point estimate model parameters.....	40
Figure 16	Representative comparison of uniform prior and posterior distributions for human (pooled mixed gender) liver microsomal metabolism parameters .....	41
Figure 17	Representative comparison of uniform prior and posterior distributions for oxidative metabolism of chloroprene in human (pooled mixed gender) lung microsomes .....	42
Figure 18	Probability frequency of chloroprene oxidative metabolism parameters in male (M) and female (F) B6C3F1 mouse liver microsomes .....	43
Figure 19	Probability frequency of chloroprene oxidative metabolism parameters in male (M) and female (F) B6C3F1 mouse lung microsomes.....	44
Figure 20	Probability frequency of chloroprene oxidative metabolism parameters in male (M) and female (F) B6C3F1 mouse kidney microsomes.....	45
Figure 21	Probability frequency of chloroprene oxidative metabolism parameters in male (M) and female (F) Fischer rat liver microsomes .....	46
Figure 22	Probability frequency of chloroprene oxidative metabolism parameters in male (M) and female (F) Fischer rat lung microsomes.....	47
Figure 23	Probability frequency of chloroprene oxidative metabolism parameters in male (M) and female (F) Fischer rat kidney microsomes .....	48
Figure 24	Distribution of chloroprene oxidative metabolism time course in male B6C3F1 mouse liver microsomes.....	49
Figure 25	Distribution of chloroprene oxidative metabolism time course in female B6C3F1 mouse liver microsomes.....	50
Figure 26	Distribution of chloroprene oxidative metabolism time course in male Fischer rat liver microsomes .....	51
Figure 27	Distribution of chloroprene oxidative metabolism time course in female Fischer rat liver microsomes .....	52
Figure 28	Distribution of chloroprene oxidative metabolism time course in male B6C3F1 mouse lung microsomes .....	53
Figure 29	Distribution of chloroprene oxidative metabolism time course in female B6C3F1 mouse lung microsomes .....	54
Figure 30	Distribution of chloroprene oxidative metabolism time course in male Fischer rat lung microsomes .....	55
Figure 31	Distribution of chloroprene oxidative metabolism time course in female Fischer rat lung microsomes .....	56
Figure 32	Distribution of chloroprene oxidative metabolism time course in male B6C3F1 mouse kidney microsomes .....	57
Figure 33	Distribution of chloroprene oxidative metabolism time course in female B6C3F1 mouse kidney microsomes .....	58
Figure 34	Distribution of chloroprene oxidative metabolism time course in male Fischer rat kidney microsomes .....	59
Figure 35	Distribution of chloroprene oxidative metabolism time course in male Fischer rat kidney microsomes .....	60



Figure 36	Distribution of chloroprene oxidative metabolism time course in human (pooled mixed gender) liver microsomes.....	61
Figure 37	Distribution of chloroprene oxidative metabolism time course in human (pooled mixed gender) lung microsomes.....	62

## LIST OF APPENDICES

	Page
Appendix A	Purity Analysis of β-Chloroprene Provided by the Sponsor’s Supplier..... 64
Appendix B	Human Kidney Microsome Data Sheet..... 67
Appendix C	Gas Chromatography Gerstel Sampler Calibration Routine ..... 69
Appendix D	Gas Chromatography Gerstel Sampler Microsomal Incubation Routine ..... 72
Appendix E	Female Rodent Liver and Lung Microsomal Incubation Data Collected at DuPont Haskell Global Centers ..... 79
Appendix F	Rodent and Human Kidney Microsomal Incubation Data Collected at DuPont Haskell Global Centers ..... 85
Appendix G	Sample Model Code for MCMC Analysis..... 94
Appendix H	Screen Capture Documentation of Model Code and Full MCMC Chain Results..... 105

## STUDY INFORMATION

Substance Tested: • β-Chloroprene  
• 2-chloro-1,3-butadiene  
• 126-99-8 (CAS Number)

Synonym(s): Chloroprene

Haskell Number: 28355

Composition: 99% β-Chloroprene (w/w)  
1000 ppm p-tertiary butyl catechol (as stabilizing agent)

Purity: >99%

Physical Characteristics: Clear liquid

Stability: The test substance appeared to be stable under the conditions of the study; no evidence of instability was observed.

Study Initiated/Completed: November 14, 2007 / (see report cover page)

Experimental Start/Termination: October 9, 2007 / December 17, 2009

In-Life Initiated/Completed: April 16, 2008 / April 21, 2009

Notebook Number(s): E-111392-AF

## SUMMARY

β-Chloroprene (chloroprene) *in vitro* oxidative metabolism was investigated to better understand species difference in metabolic rates among B6C3F1 mice, Fischer (F344) rats, and humans. Gas phase chloroprene concentrations were quantified by gas chromatography/micro-electron capture detection (GC/μECD). Metabolism parameters for chloroprene were estimated for mice, rats, and humans in several tissues (liver, lung, and kidney) in order to support the use of a previously published PBTK model of chloroprene for cross-species extrapolation of tumor risk based on target tissue dose. The parameters were estimated from experimental data for the metabolic clearance of chloroprene *in vitro*, measured in microsomal preparations. Modeling of the *in vitro* system was performed using a simple 2-compartment pharmacokinetic description of the *in vitro* system that included a non-enzymatic loss rate. Optimization of the parameter values was conducted by 2 different methods: point-estimation using the Nelder-Mead nonlinear optimization algorithm and a Bayesian statistical approach using the Markov Chain Monte Carlo algorithm. Parameter central estimates from the 2 methods were in good agreement, providing confidence in the values obtained. Estimated rates of liver metabolism based on the Bayesian approach were similar across species in terms of intrinsic clearance. The liver V<sub>max</sub>/K<sub>m</sub> (μmol/h/g microsomal protein) values were male mouse (195) > female mouse (145) ~ male rat (138) > human (122) > female rat (79). Lung V<sub>max</sub>/K<sub>m</sub> values varied substantially with male mouse (64) >> female mouse (9.7) >> male rat (1.4) ~ female rat (1.3) > human (0.3). Kidney V<sub>max</sub>/K<sub>m</sub> values were male mouse (17) >> male and female rat (3.3-4.2) > female mouse (0.08) > human (not detectable). These data indicate that the majority of chloroprene metabolism would be expected to occur in the liver followed the lung and kidney, with the rates in the latter 2 tissues showing notable species and sex differences. The Bayesian approach also provided estimates of the uncertainty in the parameters that can be used in the PBTK model to evaluate the uncertainty in risk estimates obtained with the model.

## INTRODUCTION

Chloroprene is metabolized in mammalian systems by cytochrome P450 oxidase. The objective of this study was to develop rate constants that can be used to support physiologically based toxicokinetic modeling and identify species and sex differences relative to previously collected data for male mice and rats (Himmelstein *et al.*, 2004a).<sup>(1)</sup> *In vitro* microsomal metabolism time course data collected at the DuPont Haskell facility were sent for kinetic modeling at the Hamner Institutes. A key component of this effort was to include parameter point estimation of the previous<sup>(1)</sup> and new data and apply statistical probability analysis to define parameter variation.

## STUDY DESIGN

The table below outlines the key tasks performed for this study.

Task	Species	Sex	Tissue	Endpoints
Prepare microsomes and measure metabolism	Mouse	Male	kidney	Protein concentration, Total P450, Chloroprene concentration time course by GC/μECD
		Female	liver, lung, kidney	
	Rat	Male	kidney	
		Female	liver, lung, kidney	
	Human	Pooled	kidney	
Describe in vitro model	(start with Himmelstein <i>et al.</i> , 2004) <sup>(1)</sup>			Documentation of model code
Conduct parameter point estimation	(by ACSL Optimize) <sup>a</sup>			Vmax, Km & Vmax/Km <sup>b</sup>
Conduct probability analysis	(by Markov Chain Monte Carlo analysis)			Vmax, Km & Vmax/Km <sup>c</sup>

a Included re-analysis of B6C3F1 mouse, F344 rat, and human chloroprene microsomal oxidation data for male liver and lung microsomes from Himmelstein *et al.* (2004a).

b As point estimates

c As geometric mean (GM) and standard deviation (GSD)

## MATERIALS AND METHODS

### A. Test Substance

The test substance, β-Chloroprene (chloroprene), was supplied as a clear liquid by DuPont Performance Elastomers, Pontchartrain Works (LaPlace, Louisiana, U.S.A.). A representative purity analysis provide by the sponsor is shown in Appendix A. It contained p-tertiary butyl catechol as a stabilizing agent which subsequently was removed by filtration through activated alumina under nitrogen atmosphere as described previously (Himmelstein *et al.*, 2001).<sup>(2)</sup> The purified chloroprene was stored at < -70°C under nitrogen headspace atmosphere. The test substance appeared to be stable under the conditions of the study. No evidence of instability, such as a change in color or physical state, was observed.

For metabolism experiments, vapor concentrations were prepared by adding the liquid test substance to Tedlar<sup>®</sup> bags (SKC Inc., Eighty Four, Pennsylvania, U.S.A.) containing a known volume of room air (MW 88.5365 g/mol and 0.9598 g/cm<sup>3</sup> liquid, 3.8 µL/L air for 1000 ppm). Further gas phase dilutions were made for calibration or exposure purposes. Gas tight syringes were used for the gas transfers.

## **B. Test System**

Fischer rat (F344/DuCrI) and mice (B6C3F1/CrI) were received from Charles River Laboratories, Inc., Raleigh, North Carolina. The species and strains were selected to match those used for inhalation toxicity testing by the National Toxicology Program (NTP 1998).<sup>(3)</sup> The animals were maintained in solid bottom cages with rodent chow (Certified Rodent LabDiet<sup>®</sup> 5002, PMI<sup>®</sup> Nutrition International, LLC, St. Louis, Missouri, U.S.A.) and water *ad libitum*, and acclimated for at least 7 days prior to use. Laboratory facilities were fully accredited by the Association for Assessment and Accreditation of Laboratory Animal Care (AAALAC). All procedures involving animals were reviewed by the laboratory animal care and use committee. A total of 15 female rats and 50 female mice were used for preparation of the liver and lung microsomes. A total of 15 rats/sex and 30 female mice/sex were used for preparation of kidney microsomes.

Human kidney microsomes were purchased from Xenotech (Lenexa, Kansas, U.S.A.). The vendor supplied data sheet is given in Appendix B.

## **C. Microsome Preparation**

Female mice received on October 9, 2007 were 12.7 weeks of age at the time the liver and lung microsomes were prepared. Female rats received on November 1, 2007 were 10.9 weeks when liver and lung microsomes were made. For kidney microsomes, the male and female mice and rats were received on January 29, 2009 and were 11.9 weeks of age when the microsomes were made. Lung and liver microsomes were prepared by differential centrifugation as described by Himmelstein *et al.* (2004a).<sup>(1)</sup> The microsomal preparations were analyzed for protein by the Bradford (1976)<sup>(4)</sup> method (Bio-Rad Laboratories, Hercules, California, U.S.A.). The P450 content was measured by spectrophotometry using established methods (Omura and Sato, 1964; Guengerich, 1982).<sup>(5,6)</sup> All fractions were stored at <-70°C. Stock protein (mg protein/mL) and total P450 (nmol/mg protein) are summarized in Table 1.

## **D. Gas Chromatography Analysis**

Gas chromatography (GC) was used for quantitative analysis of chloroprene. The GC method parameters are summarized in the table below. The method was similar to the one used previously except that micro-electron capture detection (µECD) was used in place of mass spectrometry single ion monitoring (Himmelstein *et al.*, 2004).<sup>(1)</sup> The µECD was used because it gave adequate sensitivity for quantitation of the parent chemical. Data on the concentration of the epoxide metabolite was not collected in the current experiments because of the focus on total chloroprene metabolism as a dosimetric for dose-response modeling (Himmelstein *et al.* 2004b).<sup>(7)</sup>

Samples were injected on the GC using a robotic x-y-z programmable multipurpose sampler (MPS2, Gerstel US, Baltimore, Maryland, U.S.A.) with a headspace injection volume of 200 µL. Calibrations were performed over a range of concentrations (0.25 – 604 ppm) and based on peak area responses for a 5-point calibration. A standard curve was generated and checked on each day of analysis.

Instrument: Agilent HP6890 equipped with Gerstel MP2 autosampler

Gerstel:

Syringe: 1 mL headspace, heated

Calibration conditions: See Appendix C

Incubation conditions: See Appendix D

Inlet:

Type: Split

Temperature: 175°C

Pressure: 4.05 psi

Split ratio: 5:1

Split flow: 21.2 mL/min

Total flow: 28.4 mL/min

Gas type: Helium

Column:

Type: JW 125-5032, 30 m x 530 µm, 1.5 µm film thickness

Mode: Constant pressure

Pressure: 4.05 psi

Nominal initial flow: 4.2 mL/min

Average velocity: 35 cm/sec

Method: Isothermal at 100°C

Detector:

Type: µECD

Temperature: 250°C

Mode: Constant makeup flow

Make-up flow: 30 mL/min

Make-up gas type: Argon (95%):methane (5%)

Retention time: Approximately 2.1 minutes

## E. Microsomal Incubations

The total volume of Gerstel 10-mL vials used for the incubations was confirmed by gravimetric displacement with water. The measurement was made on 2 occasions once for the liver and lung microsome incubations (n=10 vials) and once for the kidney microsome incubations (n=10 vials). The respective mean (±SD) weights when filled completely with water at room temperature were 11.648 (±0.222) and 11.634 (±0.051) grams. These values were used directly (without correction for the specific gravity of water) to calculate the corresponding headspace volumes less the 1.0 mL used for the incubation liquid phase.

The time course of chloroprene disappearance was measured in liver, lung and kidney microsomes using the method described in Himmelstein *et al.* (2004a).<sup>(1)</sup> Vials were prepared

with 0.1 M phosphate buffer (pH 7.4),  $\text{MgCl}_2$  (15 mM), EDTA (0.1 mM), glucose-6-phosphate (10 mM), and glucose-6-phosphate dehydrogenase (2 U/mL). Incubations were started by the addition  $\text{NADP}^+$  (0.53 mM). Control incubations were run in the absence of  $\text{NADP}^+$  by addition of an equal volume of phosphate buffer. Representative incubation conditions are given for female mouse liver (Appendix E) and for male mouse kidney (Appendix F). Microsomal protein concentrations were established from previous work (liver and lung) or experimentally for kidney microsomes (Appendix F). Definitive experiments used protein concentrations that ranged from 1-3 mg/mL. The injection volume was established during methods development. Headspace samples (200  $\mu\text{L}$ ) were injected via auto-sampler at 0, 12, 24, 36, 48, and 60 minutes. Area counts were recorded and headspace concentrations (nmol/mL) were calculated in Microsoft<sup>®</sup> Office Excel 2003.

## F. In Vitro Kinetic Model Description

A 2-compartment model modified from Himmelstein *et al.* (2004a)<sup>(1)</sup> was used to describe the time-concentration measurements of chloroprene in the headspace in the closed vial system. The current model describes the loss of chloroprene from the headspace as 1) background loss rate and 2) microsomal oxidation only (1-CEO hydrolysis pathway was turned off). To estimate the gender-specific variability of the kinetic parameters, male tissue data from Himmelstein *et al.* (2004a)<sup>(1)</sup> were re-evaluated in the parameter optimization process. For a more detailed description of the male dataset and the 2-compartment model, see Himmelstein *et al.* (2004a).<sup>(1)</sup>

## G. Kinetic Parameter Point Estimation

To quantitatively compare the more commonly used point-estimation technique with the Bayesian approach, all model parameters were optimized with ACSL-Optimize (version 11.8.4, AEgis, Technologies Group, Inc, Huntsville, Alabama, USA), using the Nelder-Mead method with a relative error minimization-based, log-likelihood function.

## H. Kinetic Parameter Probability (Bayesian) Analysis

In addition to the traditional point estimation, Bayesian analysis was performed to evaluate the uncertainty and variability of the metabolic parameters. Bayesian analysis is a statistical procedure which estimates the model parameters of an underlying distribution based on the likelihood of the previous knowledge (prior distributions) and observed data. When gender-specific tissue data were available (i.e., rat and mouse), a 2-level hierarchical Bayesian model was used to estimate the gender-variability of the metabolic parameters.<sup>a</sup>

This approach was hierarchical in the sense that the uncertain population level (species) parameters at the top level define the variability of the lower-level (gender) parameter values, which in turn predict the headspace concentrations in each experiment as a function of the initial

---

<sup>a</sup> Bayesian analysis can be implemented using a Markov chain Monte Carlo (MCMC) algorithm which updates the prior distributions based on the posterior likelihoods. For each iteration, the model proposes new values for the parameters (one at a time), re-computing the posterior likelihood. When the posterior likelihood for the new proposed value is relatively good compared to the likelihood for the current parameter values, it is more likely to be accepted. In this way, the probability of moving from one set of proposed values to another depends on how “good” the proposed values are. Better parameter values tend to be accepted more often than inferior parameter values and thus an approximation of the posterior density for the parameters is obtained.



chloroprene exposure concentration. For incubation of chloroprene with human tissue microsomes, only population-level parameters were estimated since there was only mixed gender data available. An example of the model code for one of the MCMC analyses is provided in Appendix G.

## 1. Definition of Prior Distributions

Inter-gender variability for a given microsomal activity parameter (in log-scale) was described by a normal distribution with the population mean  $M$  and the standard deviation  $S$ . The prior distribution of  $M$  was modeled by drawing  $M$  from a uniform distribution (Table 2). The same log-uniform distributions were used for  $V_{max}$ ,  $K_m$  and  $V_{max}/K_m$  for all the animal species, tissues, and doses. It was assumed that the log-uniform distribution  $[-10, 5]$ , with lower bound  $4.5e-5$  and upper bound 148, was broad enough to encompass the actual distributions of the metabolic parameters. The values were determined from the point estimation results in Himmelstein *et al.* (2004a)<sup>(1)</sup>, and 2 preliminary MCMC analyses. Before a fixed log-uniform distribution  $[-10, 5]$  was selected, 2 uniform distributions were tested for microsomal activity parameters; one  $[1e-8, 500]$  (natural scale); and the other  $[-20, 10]$  (log-scale). All 3 “prior” types produced the identical posterior results given the same variability and error model. The log-uniform  $[-10, 5]$  was chosen to reduce the sampling time.

Prior descriptions of the gender-specific variability ( $S$ ) were chosen to be lognormal  $[0.3, 5]$ . Because the MCMC parameters were sampled in log-space, the estimated gender-specific variability was an equivalent description to the coefficient of variation. One additional distribution, lognormal  $[0.3, 1]$ , was tested in the preliminary analysis. Given the same prior conditions on other parameters, the posterior results obtained from the 2 priors for gender-specific variability were very compatible. The broader prior (lognormal  $[0.3, 5]$ ) was selected to avoid over-constraining the parameters. For each gender, the individual-level parameter ( $m$ ) was sampled from the population distribution (Norm( $M, S$ )). The exponential form of the individual parameters ( $\exp(m)$ ) were then used as the inputs to compute the 2-compartment PK model predictions. The data likelihoods (likelihoods of getting the observed data given the individual parameter values) were calculated by assuming that the log-transformed predictions were normally distributed around the log-transformed  $M$  with a variance of  $\delta^2$ . The prior distribution for  $\delta$  was defined as Normal  $[1, 1]$ .

## 2. MCMC Computation Process

MCMC process is a computationally intensive search for parameter values and updating prior distributions based on posterior likelihoods. The following steps were performed in the each MCMC iteration leading to probability based estimates of  $V_{max}$ ,  $K_m$  or  $V_{max}/K_m$ :



Step	Computation
A	Sample population parameter 'M' from the prior distribution
B	Sample gender-specific variability 'S' from the prior distribution
C	Sample gender-specific parameter 'm' from Norm (M, S)
D	Calculate metabolic parameter (Vmax, Km or Vmax/Km) as exp(m)
E	Compute the model predictions with the updated model parameters
F	Compute the posterior likelihood with each new updated parameter based on their prior distributions, and the experimental data
G	Repeat steps d-f for each gender
H	Repeat steps a-g for each MCMC iteration until convergence of the posterior distributions of M and m is reached.

The method of Brooks and Gelman (1998)<sup>(8)</sup> was used to diagnose the convergence of MCMC chains. Presentation of the process included probability frequencies, mean (exp(m)) and standard deviation (std(exp(m))) estimates of the 50<sup>th</sup> percentile central tendencies, time course plots of chloroprene headspace concentrations with model estimates as a distribution of 50 simulation samples. In addition to the example MCMC model code given in Appendix G, a summary of the full MCMC file collection is presented in Appendix H.

## RESULTS AND DISCUSSION

Stock protein concentrations were highest for the liver microsomes (ranging from 25.6 to 34.6 mg/mL) with lower concentrations in the lung (6.1-8.4 mg/mL) and kidney (6.0-10.0 mg/mL) (Table 1). The P450 content likewise was highest in the liver, followed by the kidney, and non-detected levels in the lung. The non-detectable P450 content was most likely because of the lack of sensitivity of the carbon monoxide binding (spectrophotometric) assay (LOD ~ 0.02 nmol/mg protein). The stock proteins were diluted to 1-3 mg/mL of total incubation volume for studying the rate of chloroprene metabolism. Metabolic uptake (disappearance from the headspace) was initially characterized qualitatively as the percent change between the starting and final measured concentration (Appendices E-F). Human kidney microsomes were the only tissue that showed no discernable decline over the 60 minute incubation period (Appendix F). The metabolism of chloroprene could be easily detected in liver, and although at a slower rate in lung and kidney incubations as well. The concentration time course data, except for the human kidney, were determined adequate for in vitro modeling based on comparison of percent uptake relative to the control incubations (no NADP<sup>+</sup>).

A Bayesian statistical approach using the Markov Chain Monte Carlo (MCMC) algorithm was adapted to analyze in vitro chloroprene metabolism data. Nine MCMC analyses were performed for this study (control dataset for background loss rate; liver, lung, and kidney for rat and mouse, and liver and lung for human), using the “prior” distributions summarized in Table 2. The human kidney microsomal metabolism data was not modeled because of the failure to produce experimentally measurable chloroprene uptake. Three MCMC chains were run for each analysis. A minimum of 200,000 iterations were performed for each chain. The first 100,000 iterations were used to initialize the Monte Carlo chain, and these results were used as the starting point for completion of the remaining 100,000 iterations. Once the MCMC chains converged to a stationary distribution, the “converged” parts of the chains were considered representative samples from the posterior distributions. The MCMC chains were considered converged when the estimates of the corrected scale reduction factor (CSRF) were close to 1; a value of 1.2 was selected as a cut-point for determining convergence. The CSRF values (abbreviated as R in the model) for all the parameters were below 1.1. After the chains converged, 4000 sets of the parameters were randomly sampled from the converged part of the chains to represent the posterior distributions. Intrinsic clearance ( $V_{max}/K_m$ ) was calculated from the geometric mean values for  $V_{max}$  and  $K_m$ .

The posterior distribution for the background loss rate (in addition to removal of chloroprene during headspace sample extraction) was based on 8 sets of control data (the complete female data set plus the male kidney dataset). A prerequisite assumption was that the in vitro experimental background loss rate was independent of gender, tissue, and dose. The first-order rate constant included in the model to account for the background loss was based on the resulting posterior distribution [95<sup>th</sup>, 50<sup>th</sup> and 5<sup>th</sup> percentile of 1.5, 1.4, and 1.3 L/hr/g, respectively].

For comparison with the Bayesian analysis, the traditional Nelder-Mead optimization routine for model parameter optimization was run using ACSL-Optimize. The point estimate of the background loss rate was 1.41 L/hr/g using ACSL-Optimize. The point estimation results for microsomal oxidation parameters with and without background loss rate are presented in

Tables 3 and 4, respectively. Even with the background loss rate, microsomal oxidation was still predicted to occur in most of the tissues. In some of the low metabolism tissues it was possible to see an impact of considering the background loss; for example the estimated intrinsic clearance dropped from 1.3 to 0.9 L/hr/g in the male rat lung microsomal incubations. The greatest impact was for the female mouse kidney where the intrinsic clearance dropped from 0.83 to 0.024 L/hr/g, which was essentially negligible. Figures 2-15 show the comparison of chloroprene headspace measurements and predictions simulated using point estimates of the model parameters (Table 4).

Posterior distributions of the model parameters showed excellent agreement with the point estimates (Table 4). The point estimates were typically within one standard deviation of the MCMC mean values (Table 5), providing a cross-validation between the 2 optimization techniques. One exception was for  $V_{max}/K_m$  in the human lung, where the Bayesian estimate (0.3) was somewhat lower than the point estimate (0.9). The uncertainties in the model parameters were significantly reduced from the prior distributions (Figures 16 and 17) demonstrated by the narrow posterior distribution. For all species, microsomal activities were highest in the liver, followed by lung or kidney (Tables 4 and 5). Gender differences in the estimated parameter values were observed in all tissues for which the necessary data were available (Table 4); for example, the intrinsic clearance ( $V_{max}/K_m$ ) for liver microsomes was higher in male than female animals for both rats and mice. Figures 18-23 compare the posterior distributions of metabolic parameters in male and female. Species differences on the tissue intrinsic clearance rates were also observed. Higher clearance was estimated in microsomal incubation with the lung than kidney for mice; but this was reversed for rats (Table 4 and 5). Figures 24-37 present the distributions of chloroprene predictions simulated using model parameters randomly drawn from their posterior distributions. The width of the band showing 50 randomly selected simulations reflects the impact of the uncertainty and variability of the metabolic parameters on the distribution of the model output (chloroprene concentration). As a result the point estimate and Bayesian approaches gave simulations that well represent the experimental in vitro concentration time course data (Figures 2-15 and 24-37) with the latter approach providing estimates of parameter uncertainty.

## CONCLUSIONS

Metabolism parameters for chloroprene were estimated for mice, rats, and humans in several tissues (liver, lung, and kidney) in order to support the use of a previously published PBTK model of chloroprene for cross-species extrapolation of tumor risk based on target tissue dose. The parameters were estimated from experimental data for the metabolic clearance of chloroprene in vitro, measured in microsomal preparations. Modeling of the in vitro system was performed using a simple 2-compartment pharmacokinetic description of the in vitro system that included a non-enzymatic loss rate. Optimization of the parameter values was conducted by 2 different methods: point-estimation using the Nelder-Mead nonlinear optimization algorithm and a Bayesian statistical approach using the Markov Chain Monte Carlo algorithm. Parameter central estimates from the 2 methods were in good agreement, providing confidence in the values obtained. Estimated rates of liver metabolism based on the Bayesian approach were similar across species in terms of intrinsic clearance. The liver  $V_{max}/K_m$  ( $\mu\text{mol/h/g}$  microsomal protein) values were male mouse (195) > female mouse (145) ~ male rat (138) > human (122) >

female rat (79). Lung Vmax/Km values varied substantially with male mouse (64) >> female mouse (9.7) >> male rat (1.4) ~ female rat (1.3) > human (0.3). Kidney Vmax/Km values were male mouse (17) >> male and female rat (3.3-4.2) > female mouse (0.08) > human (not detectable). These data indicate that the majority of chloroprene metabolism would be expected to occur in the liver followed the lung and kidney, with the rates in the latter 2 tissues showing notable species and sex differences. The Bayesian approach also provided estimates of the uncertainty in the parameters that can be used in the PBTK model to evaluate the uncertainty in risk estimates obtained with the model.

## RECORDS AND SAMPLE STORAGE

Specimens (if applicable), raw data, the protocol, amendments (if any), and the final report will be retained at DuPont Haskell, Newark, Delaware, Iron Mountain Records Management, Wilmington, Delaware, or Quality Associates Incorporated, Fulton, Maryland.

Laboratory-specific raw data such as personnel files, instrument, equipment, refrigerator and/or freezer raw data will be retained at the facility where the work was done.

## REFERENCES

1. Himmelstein, M.W., Carpenter, S.C., and Hinderliter, P.M. (2004a). Kinetic modeling of  $\beta$ -chloroprene metabolism: I. *In vitro* rates in liver and lung tissue fractions from mice, rats, hamsters, and humans. *Toxicol. Sci.* **79**, 18-27.
2. Himmelstein, M.W., Carpenter, S.C., Hinderliter, P.M., Snow, T.A., and Valentine, R. (2001). The metabolism of  $\beta$ -chloroprene: preliminary in vitro studies using liver microsomes, *Chem.-Biol. Interact.* 135–136, 267–284.
3. NTP (1998). Toxicology and carcinogenesis studies of chloroprene (CAS 126-99-8) in F344/N Rats and B6C3F1 Mice (Inhalation Studies), Technical Report 467, NIH Publication 98-3957, National Institutes of Health, Bethesda.
4. Bradford M.M. (1976). A rapid and sensitive method for the quantitation of microgram quantities of protein utilizing the principle of protein-dye binding. *Anal Biochem* **72**, 248-254.
5. Omura, T., and Sato, R. (1964). The carbon monoxide-binding pigment of liver microsomes. I. Evidence for its hemoprotein nature. *J. Biol. Chem.* **239**, 2370-2378.
6. Guengerich, F.P. (1982). Microsomal enzymes involved in toxicology – analysis and separation. *Principles and Methods of Toxicology* (A.W. Hayes, ed.). Raven Press, New York.
7. Himmelstein, M.W., Carpenter, S.C., Evans, M.V., Hinderliter, P.M., and Kenyon, E.M. (2004b). Kinetic modeling of  $\beta$ -chloroprene metabolism: II. The application of physiologically based modeling for cancer dose response analysis. *Toxicol. Sci.* **79**, 28-37.

8. Brooks, S.P., and Gelman, A. (1998). General methods for monitoring convergence of iterative simulations. *Journal of Computational and Graphical Statistics* 7, 434-455.

**TABLES**

Table 1  
Stock microsomal protein concentrations and screen for total P450 protein

Species	Sex	Tissue	Stock protein (mg/mL)	P450 (nmol/ mg protein)
B6C3F1 mouse	Male	Kidney	6.945	0.197
	Female	Liver	34.648	0.445
		Lung	8.429	ND
		Kidney	5.965	ND
F344 rat	Male	Kidney	9.826	0.022, 0.128 <sup>a</sup>
	Female	Liver	25.555	0.519
		Lung	6.118	ND
		Kidney	9.514	0.048
Human	Mixed	Kidney	10.0 <sup>b</sup>	ND

ND - not detected

a Measurement taken on separate days indicated variation in spectral analysis.

b Concentration provided by Xenotech

Table 2  
In vitro chloroprene metabolism prior distributions

Parameter application	Vmax, Km, Vmax/Km <sup>a</sup>	
	Distribution	Truncation
Population (exp(M))	Uniform	[4.5e-5, 150]
Gender variability (S)	Lognormal (0.3, 5)	[0.01, 10]
Individual <sup>b</sup> (exp(m))	Exp(Normal (M, S))	[2e-9, 2e4]

M - Mean; exp(M) - exponent of mean, S - standard deviation

a Units: Vmax (μmol/h/mg), Km (μmol/L), Vmax/Km (L/hr/g protein)

b Individual level parameter referred to male-specific and female-specific metabolic parameter in the 2-compartment PK model

Table 3  
Point estimate values for the microsomal oxidation of chloroprene without correction for  
background loss

Species	Sex	Tissue	Activity of microsomal oxidation <sup>a,b</sup>		
			Vmax	Km	Vmax/Km
B6C3F1 mouse	Male	Liver	0.23	1.03	224
		Lung	0.10	1.5	66.7
		Kidney	0.0137	0.73	18.8
	Female	Liver	0.12	0.9	133
		Lung	0.03	2.81	11
		Kidney	0.0015	1.81	0.83
F344 rat	Male	Liver	0.078	0.53	146
		Lung			1.3
		Kidney	0.0057	1.87	3.05
	Female	Liver	0.062	0.57	109
		Lung			2.6
		Kidney	0.0022	0.37	5.95
Human	Mixed	Liver	0.1	1.5	101
		Lung			1.3

a Obtained by ACSL Optimization

b Vmax (μmol/h/mg); Km (μmol/L); Vmax/Km (L/hr/g)



Table 4  
Point estimate values for the microsomal oxidation of chloroprene with correction for  
background loss

Species	Sex	Tissue	Activity of microsomal oxidation <sup>a,b</sup>		
			Vmax	Km	Vmax/Km
B6C3F1 mouse	Male	Liver	0.26	1.36	186
		Lung	0.13	2.0	64
		Kidney	0.01	0.5	20
	Female	Liver	0.09	0.53	174
		Lung	0.025	2.78	8.9
		Kidney	0.00004	1.7	0.024
F344 rat	Male	Liver	0.077	0.56	139
		Lung			0.9
		Kidney	0.0027	0.92	3
	Female	Liver	0.068	0.82	82
		Lung			1.2
		Kidney	0.00177	0.37	4.7
Human	Mixed	Liver	0.054	0.45	120
		Lung			0.9

a Obtained by ACSL Optimization and includes correction for background loss of chloroprene during the incubation

b Vmax (μmol/h/mg); Km (μmol/L); Vmax/Km (L/hr/g)

Table 5  
Probability analysis of microsomal oxidation parameters for chloroprene

Species	Sex	Tissue	Activity of microsomal oxidation <sup>a</sup>					
			Vmax <sup>b</sup>		Km <sup>b</sup>		Vmax/Km <sup>c</sup>	
			Mean	SD	Mean	SD	Mean	SD <sup>d</sup>
B6C3F1 mouse	Male	Liver	0.27	0.010	1.37	0.08	194.7	14.2
		Lung	0.14	0.007	2.23	0.14	63.7	5.0
		Kidney	0.013	0.001	0.77	0.08	16.8	2.3
	Female	Liver	0.123	0.010	0.85	0.12	144.5	23.0
		Lung	0.026	0.010	2.68	1.29	9.7	6.0
		Kidney	0.0003	0.0013	3.74	20.8	0.08	0.57
F344 rat	Male	Liver	0.077	0.002	0.56	0.03	138.0	7.9
		Lung					1.4 <sup>e</sup>	0.2
		Kidney	0.0025	0.0003	0.77	0.12	3.3	0.6
	Female	Liver	0.076	0.004	0.97	0.06	78.6	6.8
		Lung					1.3 <sup>e</sup>	0.2
		Kidney	0.0025	0.0003	0.60	0.08	4.2	0.7
Human	Mixed	Liver	0.055	0.001	0.45	0.02	122.2	4.8
		Lung					0.33 <sup>e</sup>	0.22
		Kidney					ND <sup>f</sup>	

a Mean (exp(m)) and standard deviation SD (exp(s)) values obtained by Markov Chain Monte Carlo (MCMC) analysis and includes correction for background loss of chloroprene during the incubation

b Vmax (μmol/h/mg); Km (μmol/L)

c Vmax/Km (L/hr/g) calculated as Vmax/Km\*1000 mg/g (unit conversion)

d Except as noted, SD = Vmax/Km \* Squareroot(({Vmax SD/Mean}<sup>2</sup>+{Km SD/Mean}<sup>2</sup>) (Taylor, J.R. (1982). An Introduction to Error Analysis: The Study of Uncertainties in Physical Measurements. University Science Books, Mill Valley.)

e Mean and SD Vmax/Km estimated directly via MCMC analysis

f ND - metabolism not detected

## FIGURES

## FIGURES

## EXPLANATORY NOTES

### ABBREVIATIONS:

Frequenc - frequency

Figure 1  
Representative gas chromatography headspace calibration curve

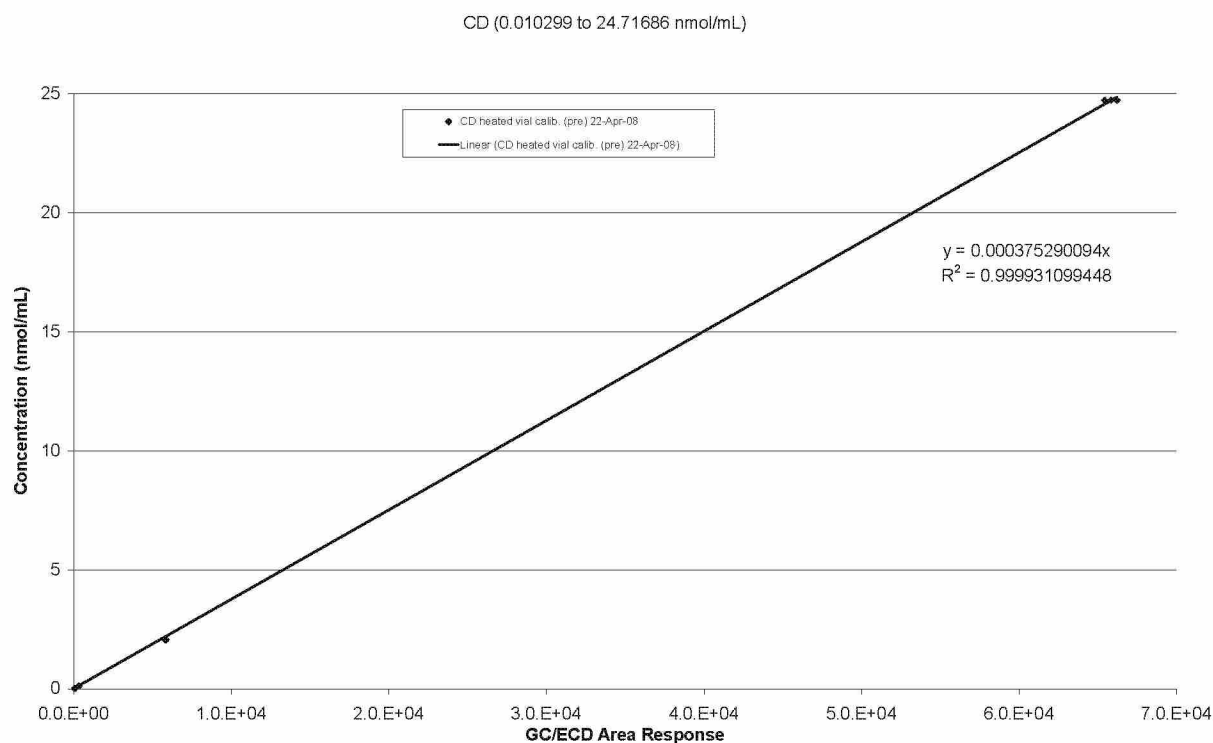
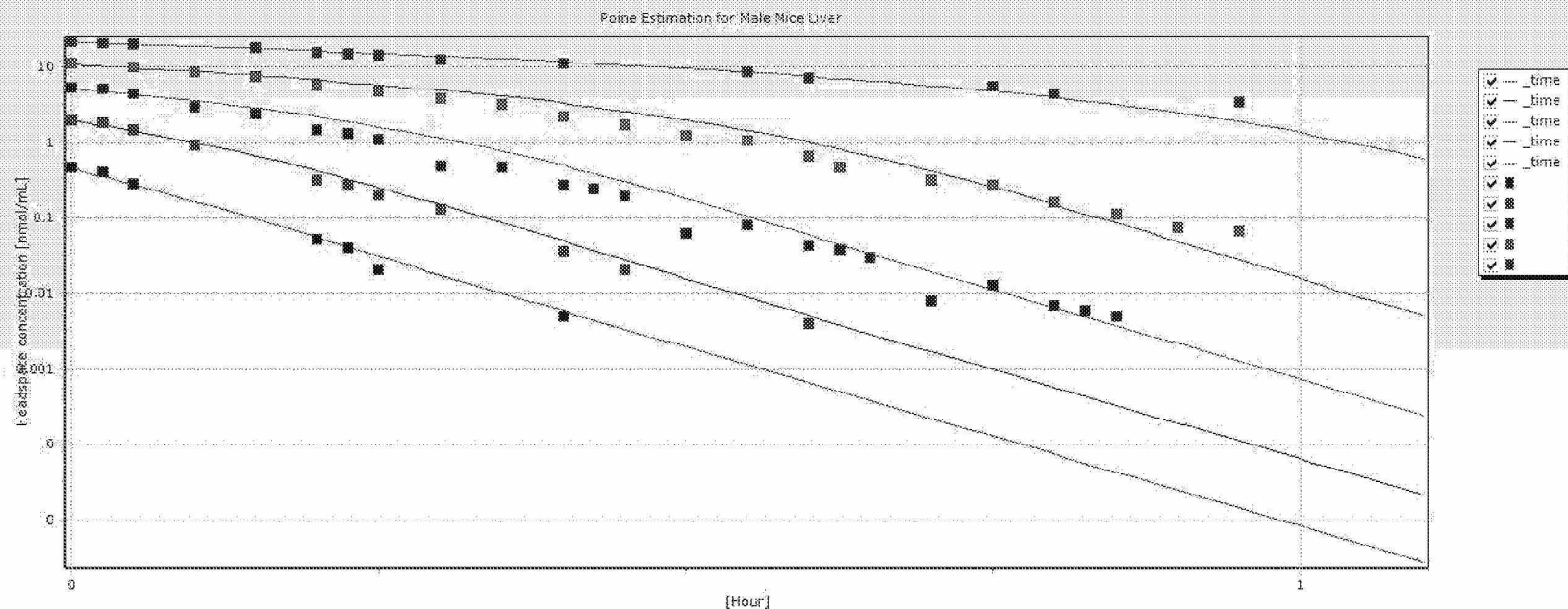
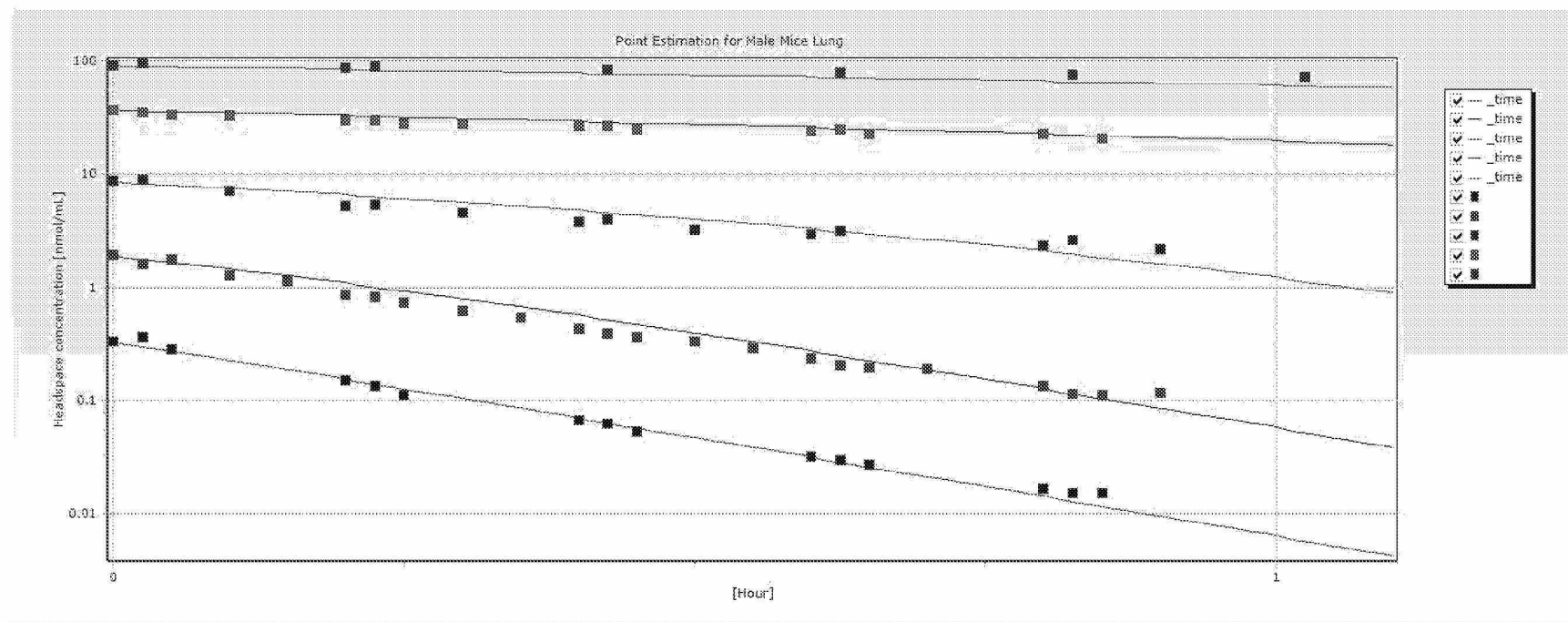


Figure 2



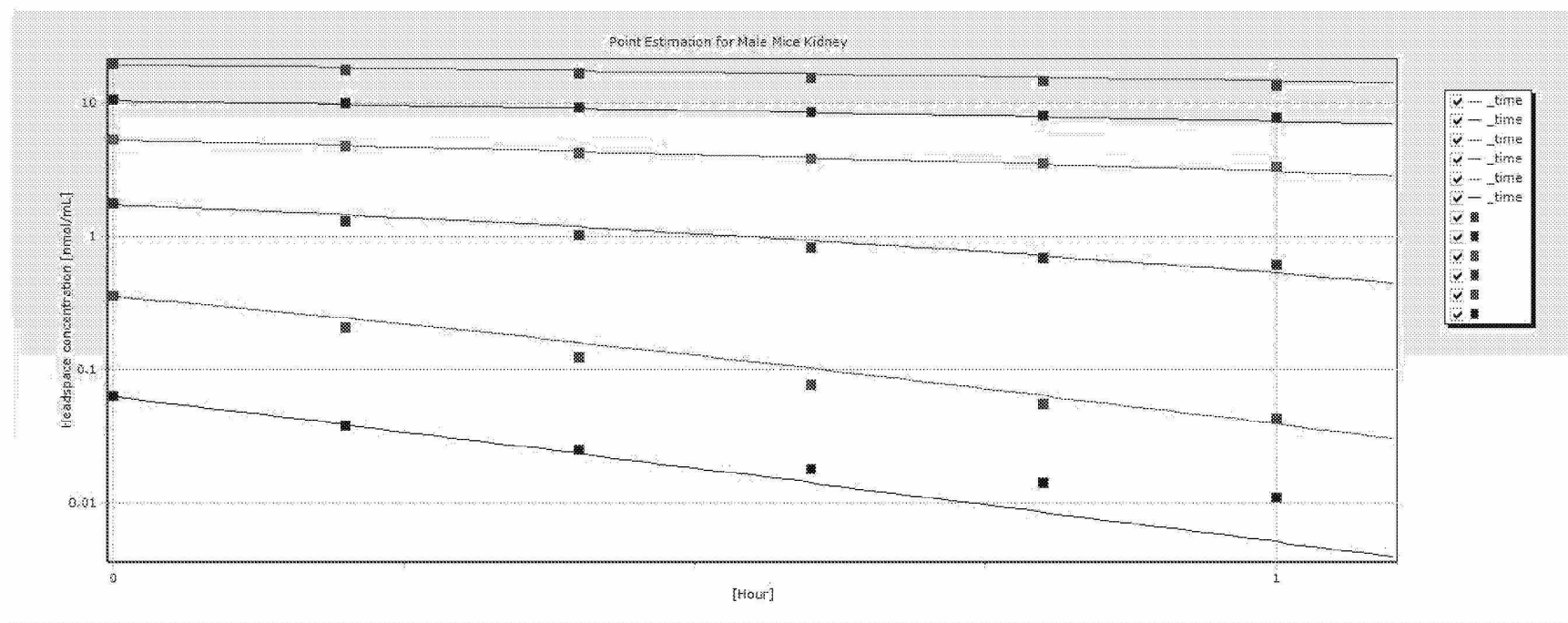
Note: Chloroprene headspace concentrations (symbols) and model simulations (lines) based on parameter values reported in Table 4.

Figure 3  
Chloroprene oxidative metabolism time course in male B6C3F1 mouse lung microsomes using point estimate model parameters



Note: Chloroprene headspace concentrations (symbols) and model simulations (lines) based on parameter values reported in Table 4.

Figure 4  
Chloroprene oxidative metabolism time course in male B6C3F1 mouse kidney microsomes using point estimate model parameters

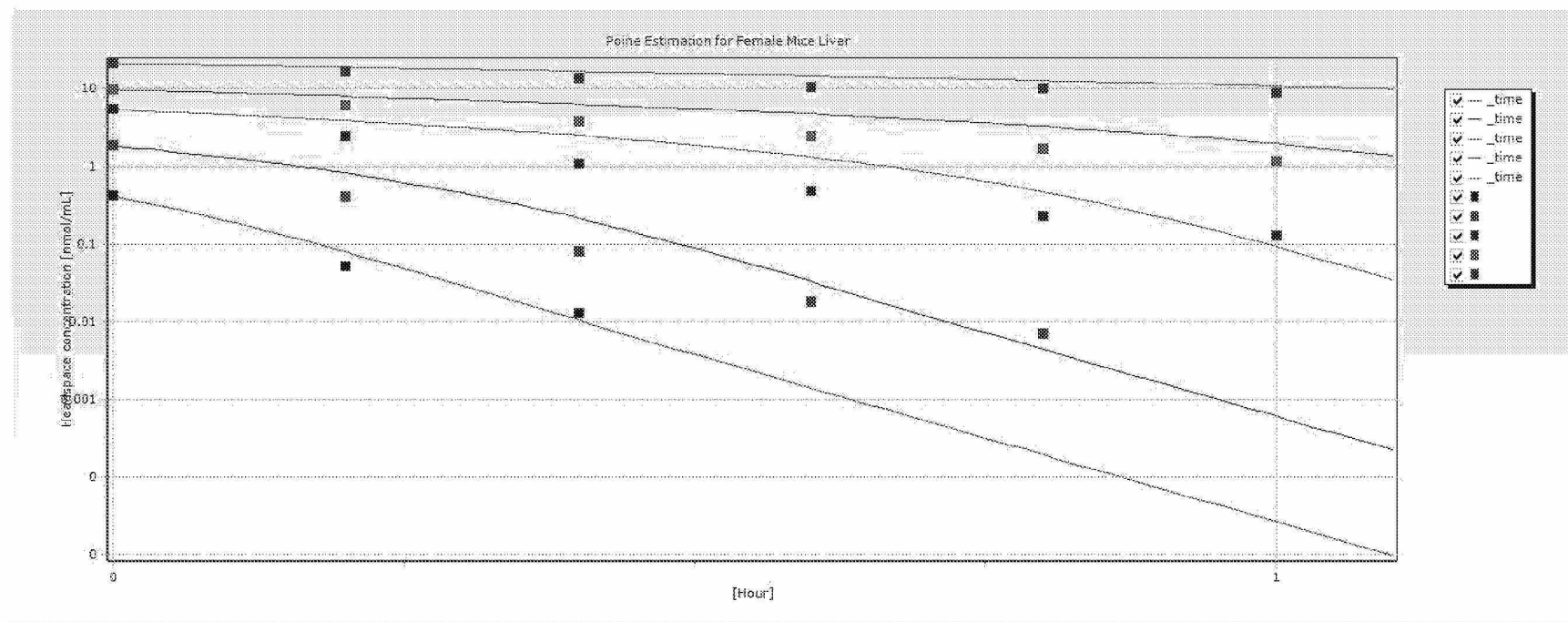


Note: Chloroprene headspace concentrations (symbols) and model simulations (lines) based on parameter values reported in Table 4.



Figure 5

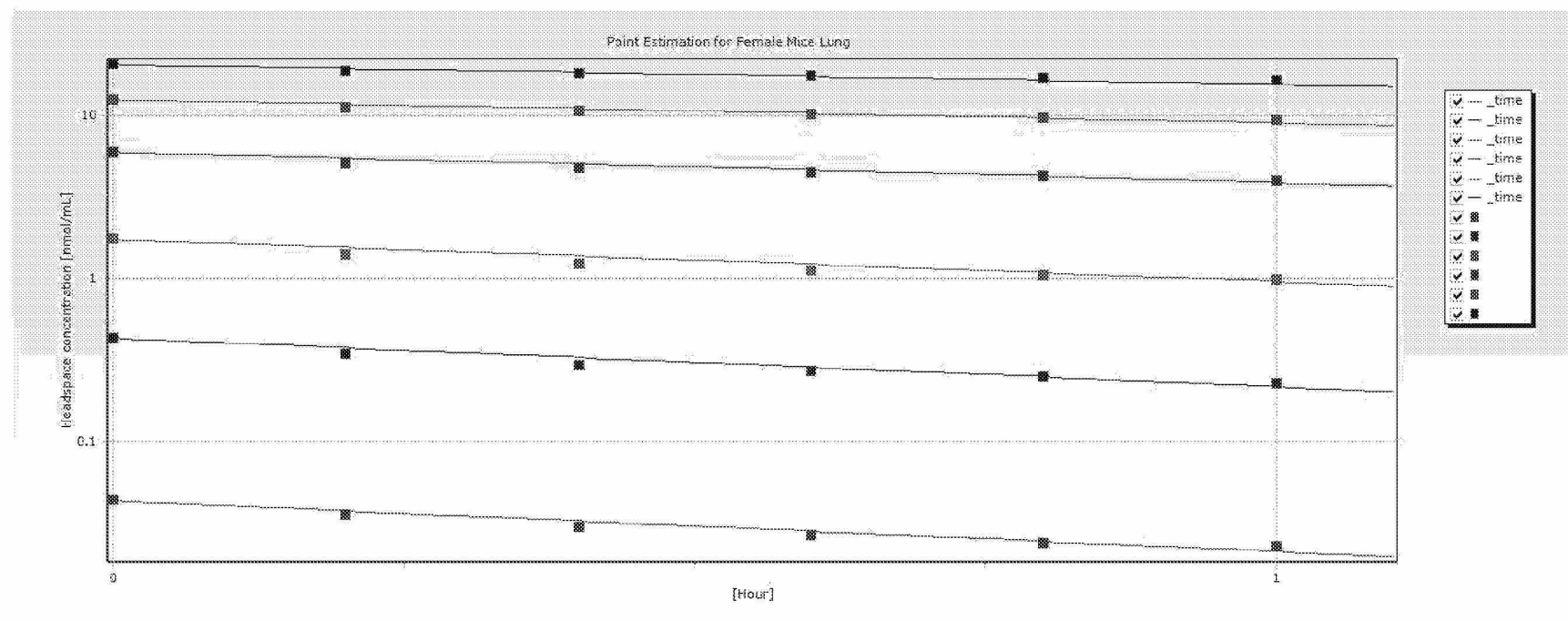
Chloroprene oxidative metabolism time course in female B6C3F1 mouse liver microsomes using point estimate model parameters



Note: Chloroprene headspace concentrations (symbols) and model simulations (lines) based on parameter values reported in Table 4.

Figure 6

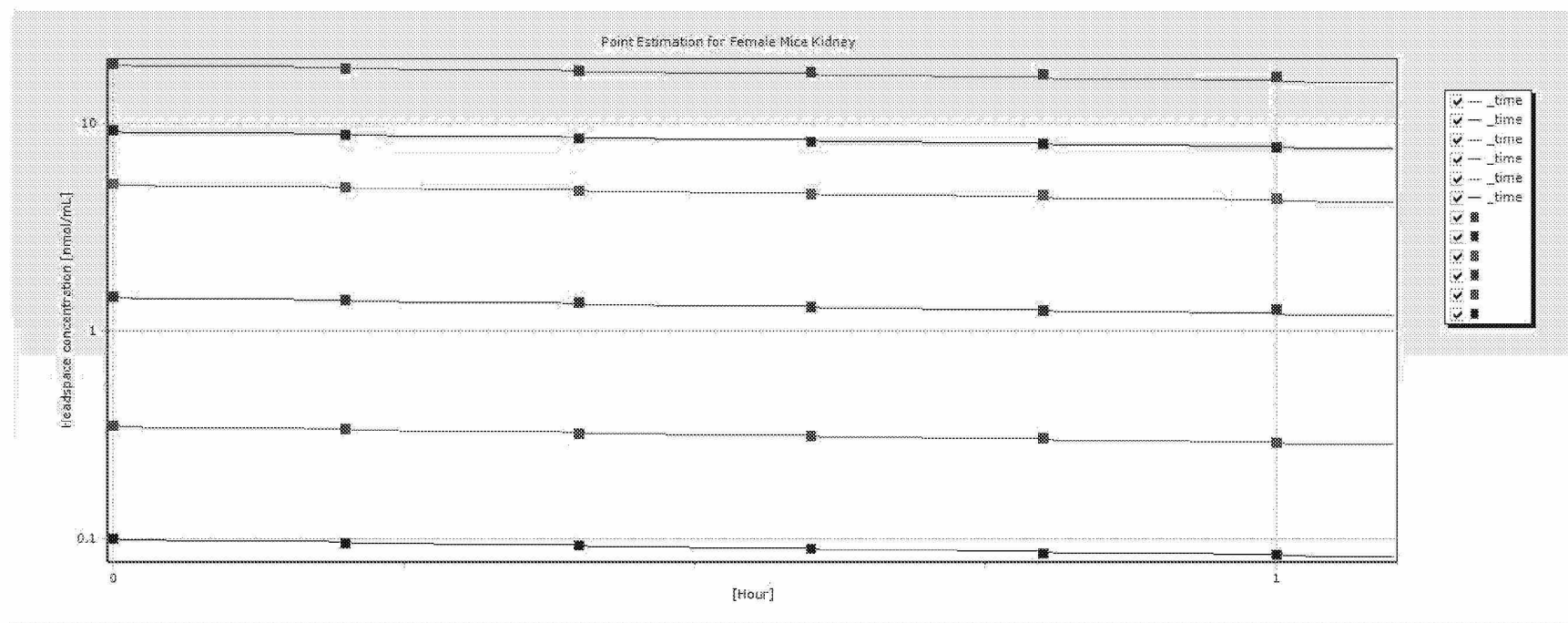
Chloroprene oxidative metabolism time course in female B6C3F1 mouse lung microsomes using point estimate model parameters



Note: Chloroprene headspace concentrations (symbols) and model simulations (lines) based on parameter values reported in Table 4.

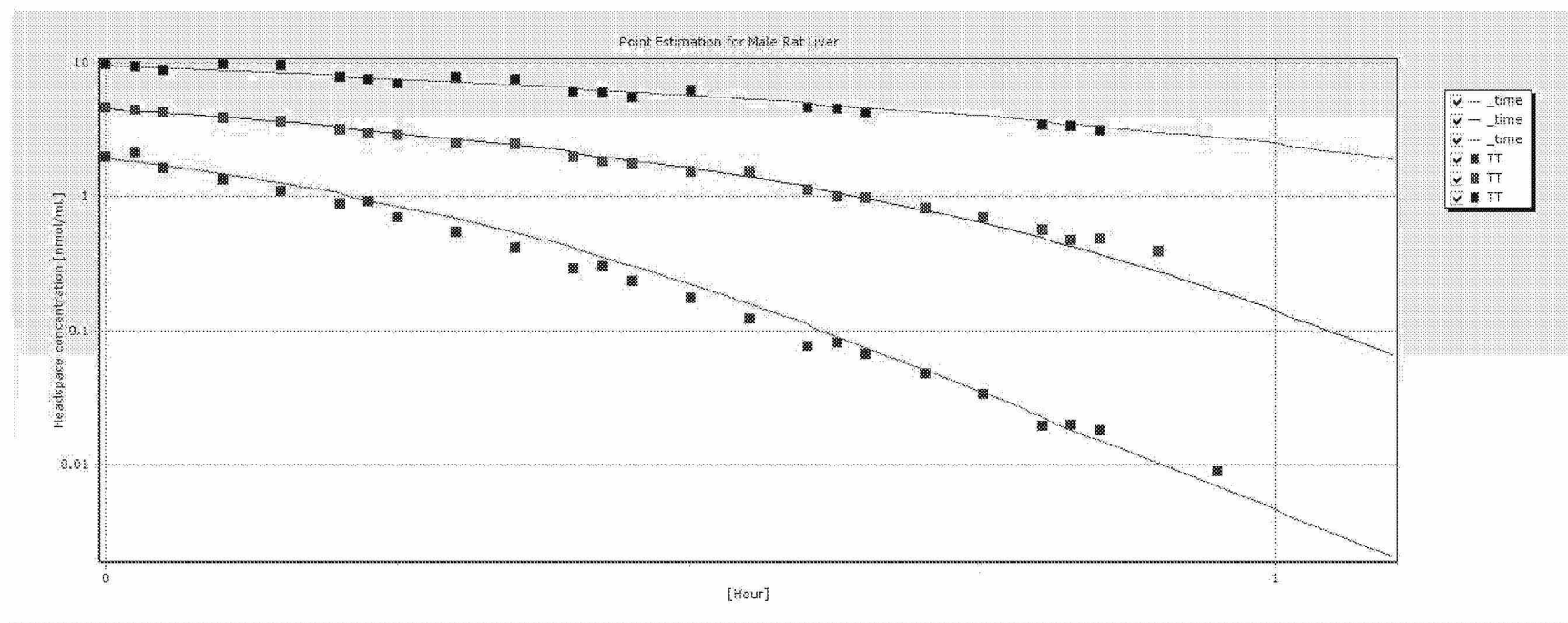
Figure 7

Chloroprene oxidative metabolism time course in female B6C3F1 mouse kidney microsomes using point estimate model parameters



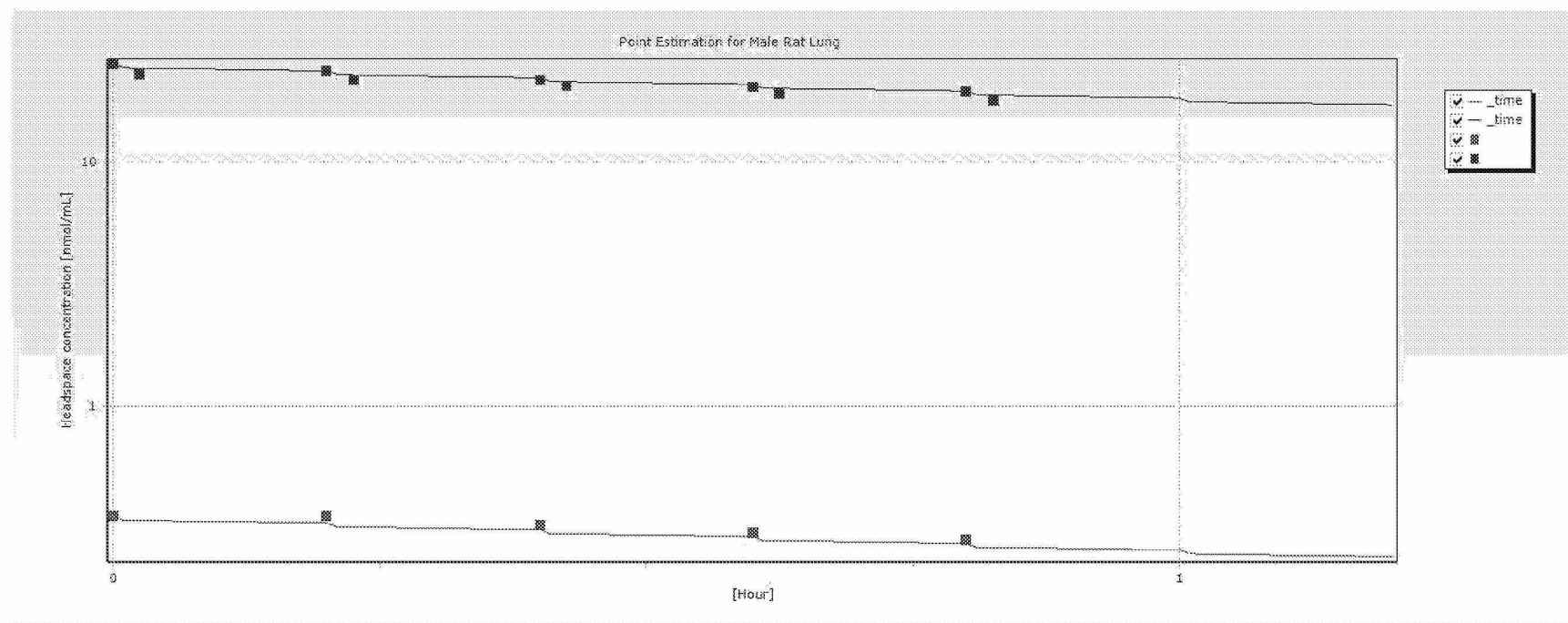
Note: Chloroprene headspace concentrations (symbols) and model simulations (lines) based on parameter values reported in Table 4.

Figure 8  
Chloroprene oxidative metabolism time course in male Fischer rat liver microsomes using point estimate model parameters



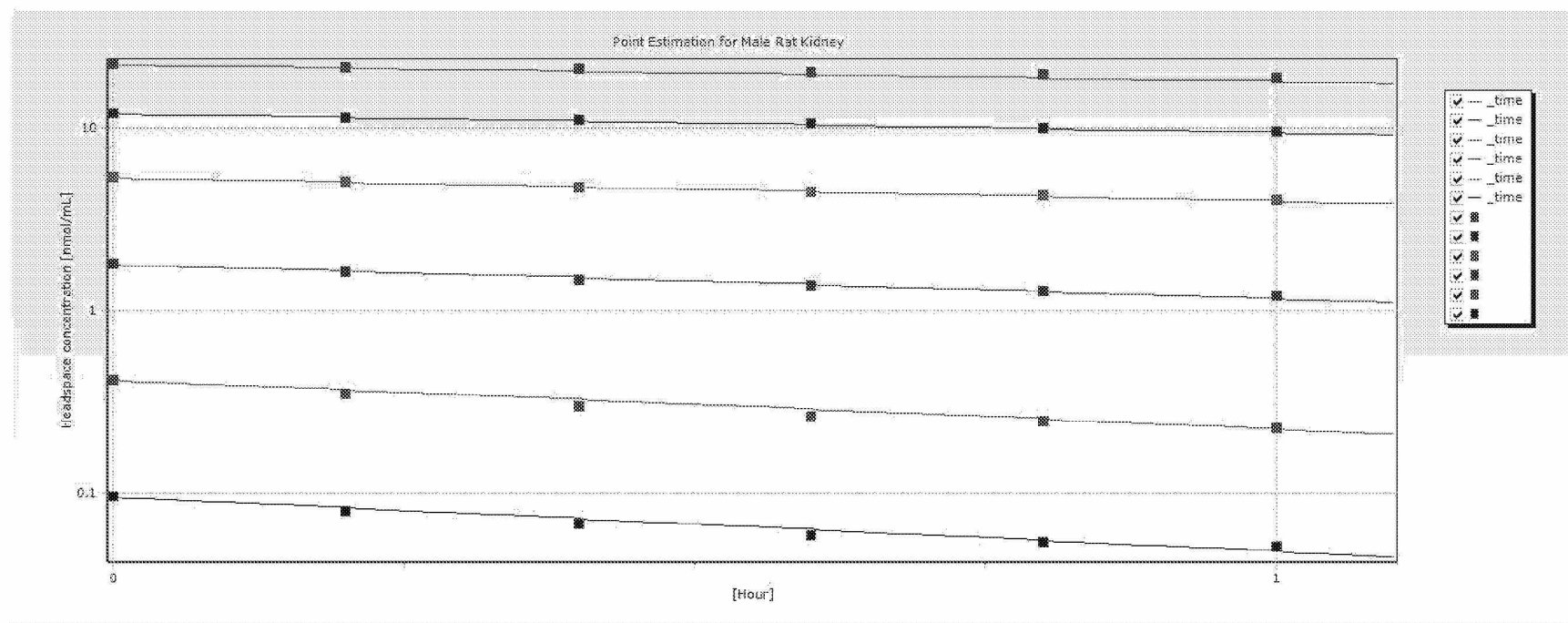
Note: Chloroprene headspace concentrations (symbols) and model simulations (lines) based on parameter values reported in Table 4.

Figure 9  
Chloroprene oxidative metabolism time course in male Fischer rat lung microsomes using point estimate model parameters



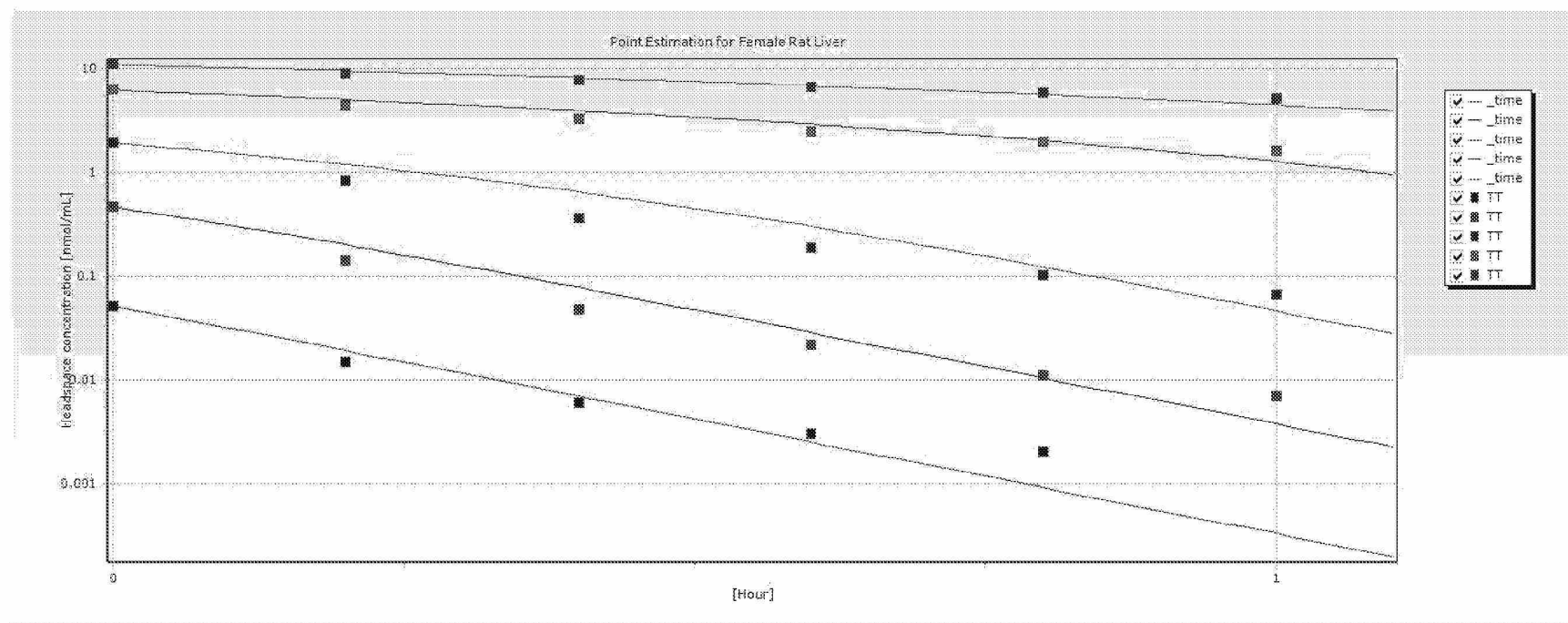
Note: Chloroprene headspace concentrations (symbols) and model simulations (lines) based on parameter values reported in Table 4.

Figure 10  
Chloroprene oxidative metabolism time course in male Fischer rat kidney microsomes using point estimate model parameters



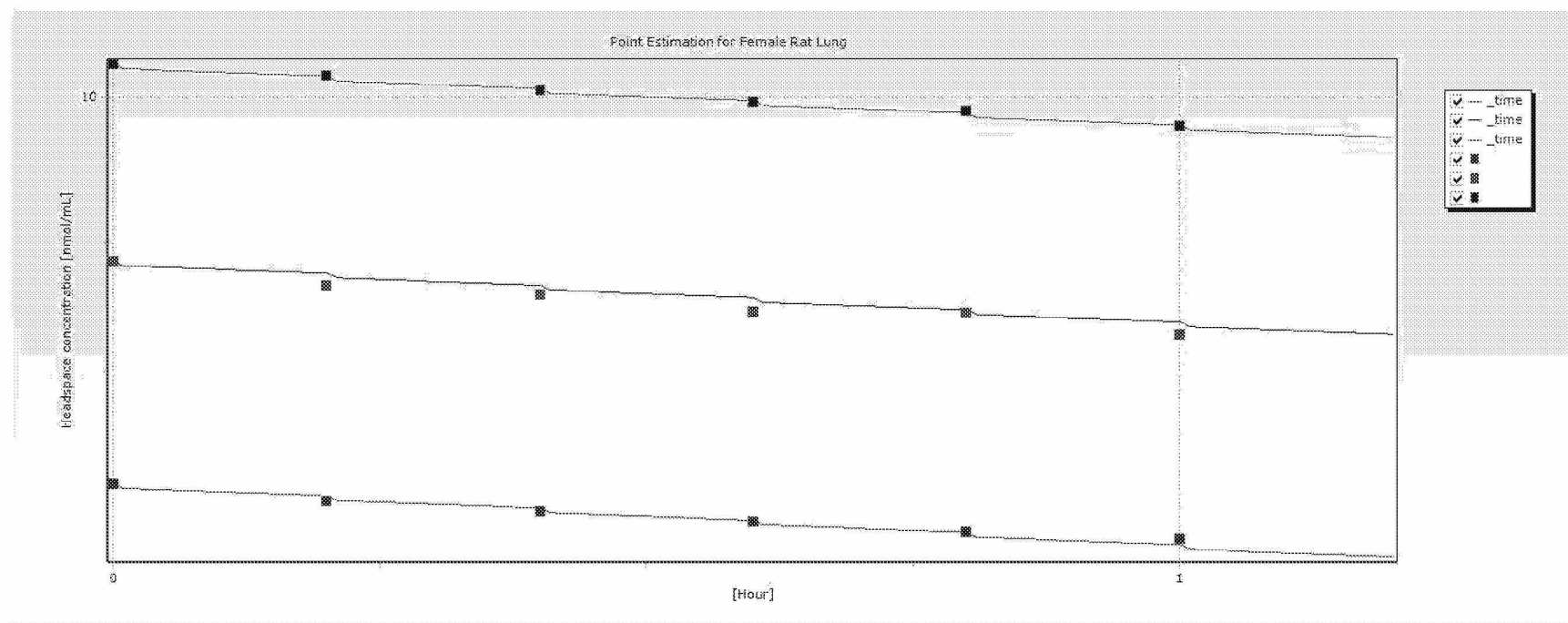
Note: Chloroprene headspace concentrations (symbols) and model simulations (lines) based on parameter values reported in Table 4.

Figure 11  
Chloroprene oxidative metabolism time course in female Fischer rat liver microsomes using point estimate model parameters



Note: Chloroprene headspace concentrations (symbols) and model simulations (lines) based on parameter values reported in Table 4.

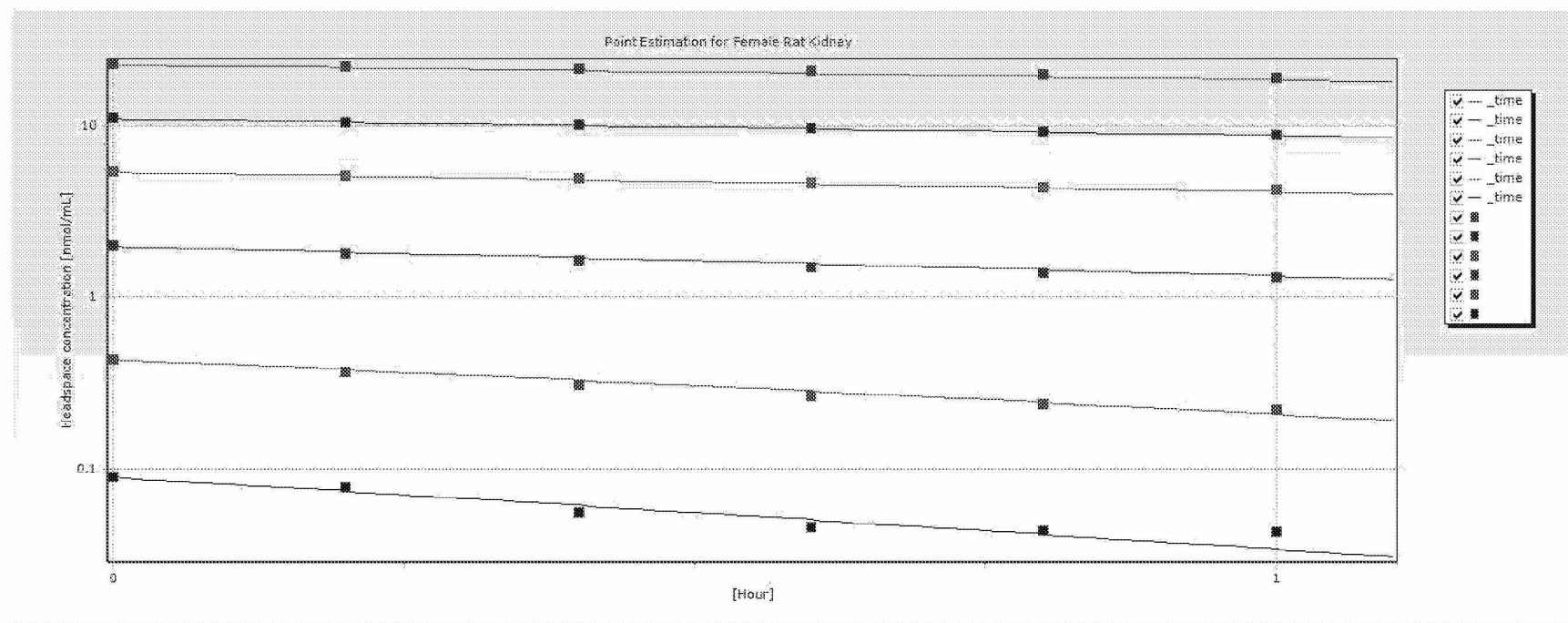
Figure 12  
Chloroprene oxidative metabolism time course in female Fischer rat lung microsomes using point estimate model parameters



Note: Chloroprene headspace concentrations (symbols) and model simulations (lines) based on parameter values reported in Table 4.

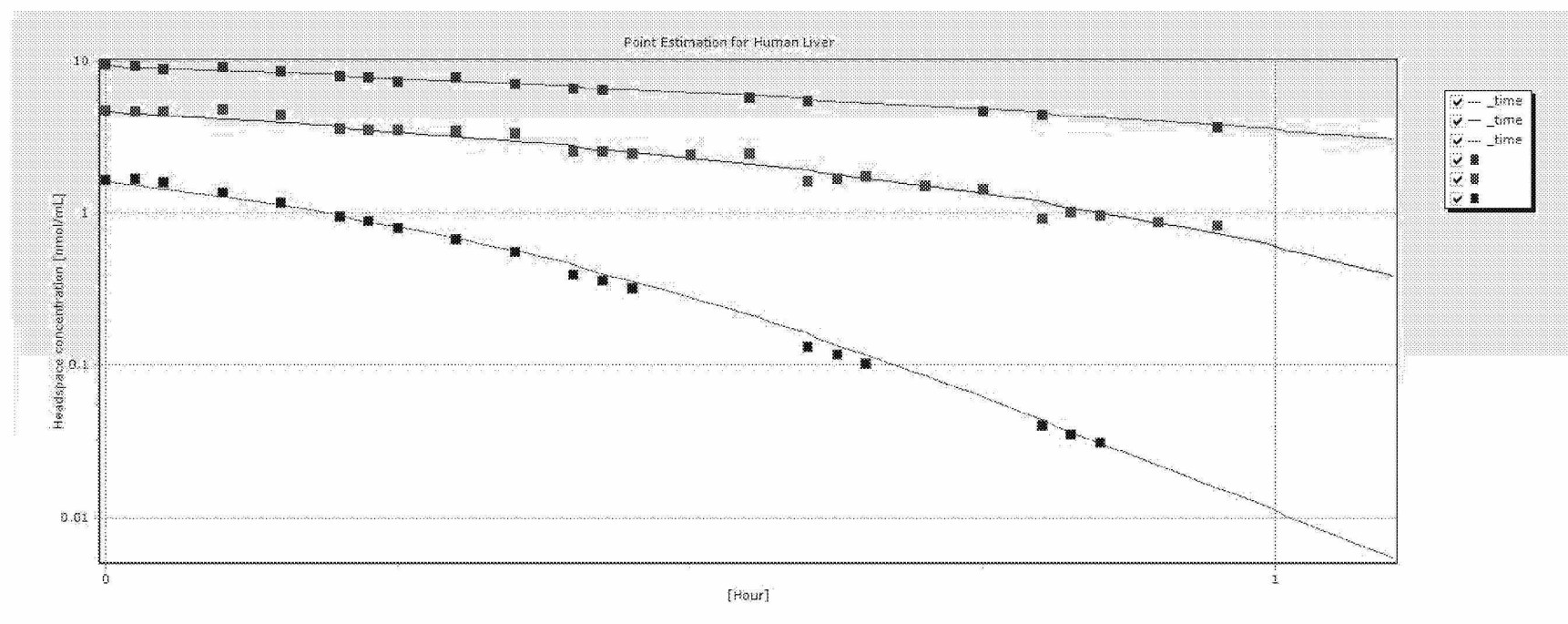


Figure 13  
Chloroprene oxidative metabolism time course in female Fischer rat kidney microsomes using point estimate model parameters



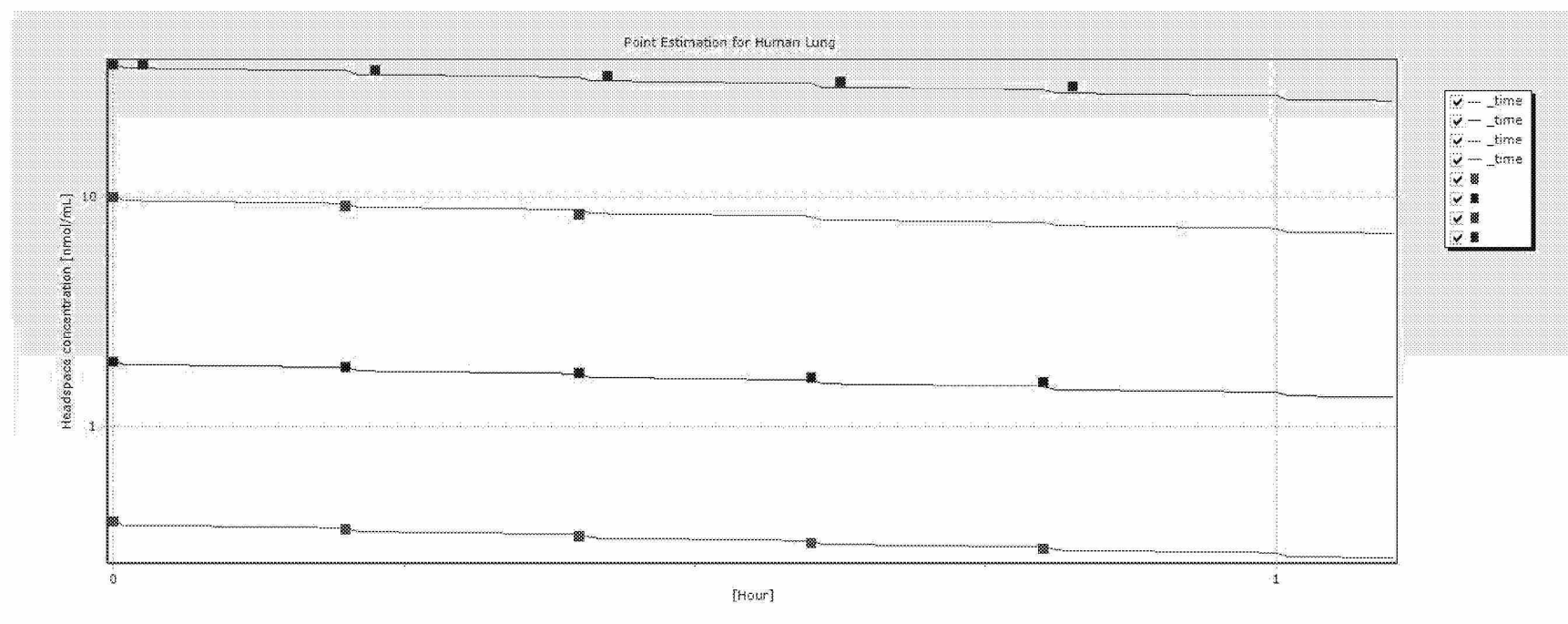
Note: Chloroprene headspace concentrations (symbols) and model simulations (lines) based on parameter values reported in Table 4.

Figure 14  
Chloroprene oxidative metabolism time course in human (pooled mixed gender) liver microsomes using point estimate model parameters



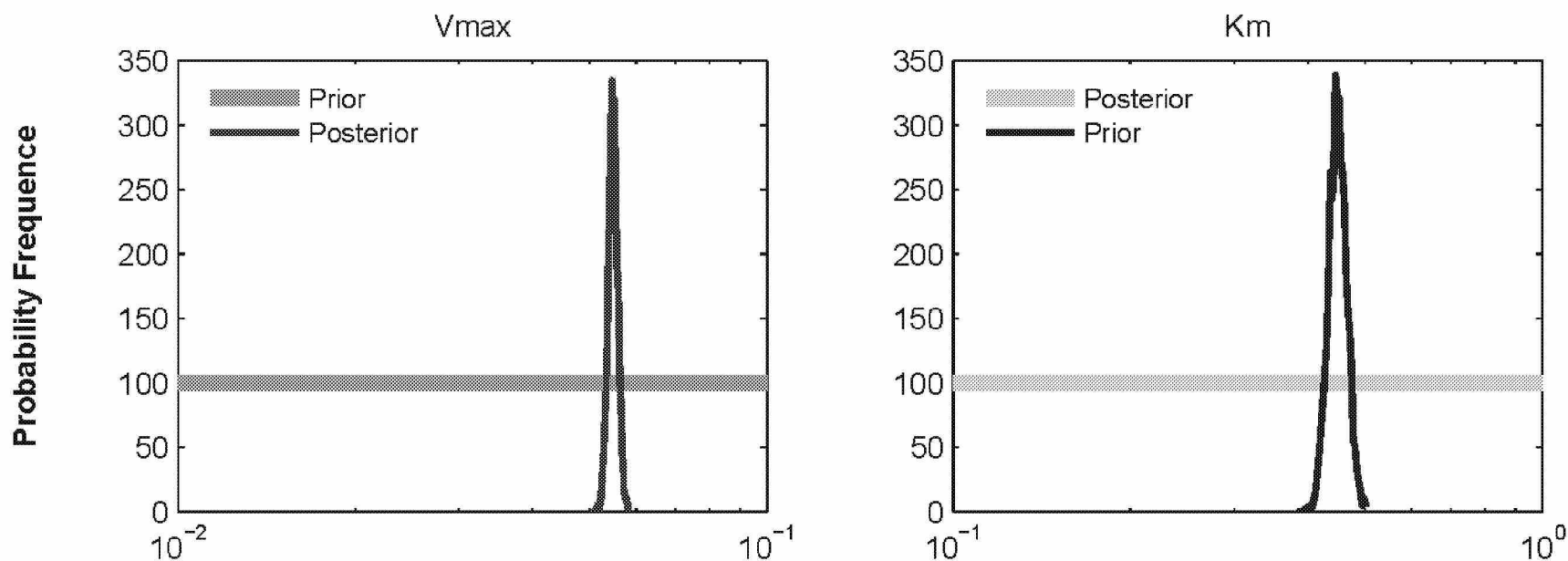
Note: Chloroprene headspace concentrations (symbols) and model simulations (lines) based on parameter values reported in Table 4.

Figure 15  
Chloroprene oxidative metabolism time course in human (pooled mixed gender) lung microsomes using point estimate model  
parameters



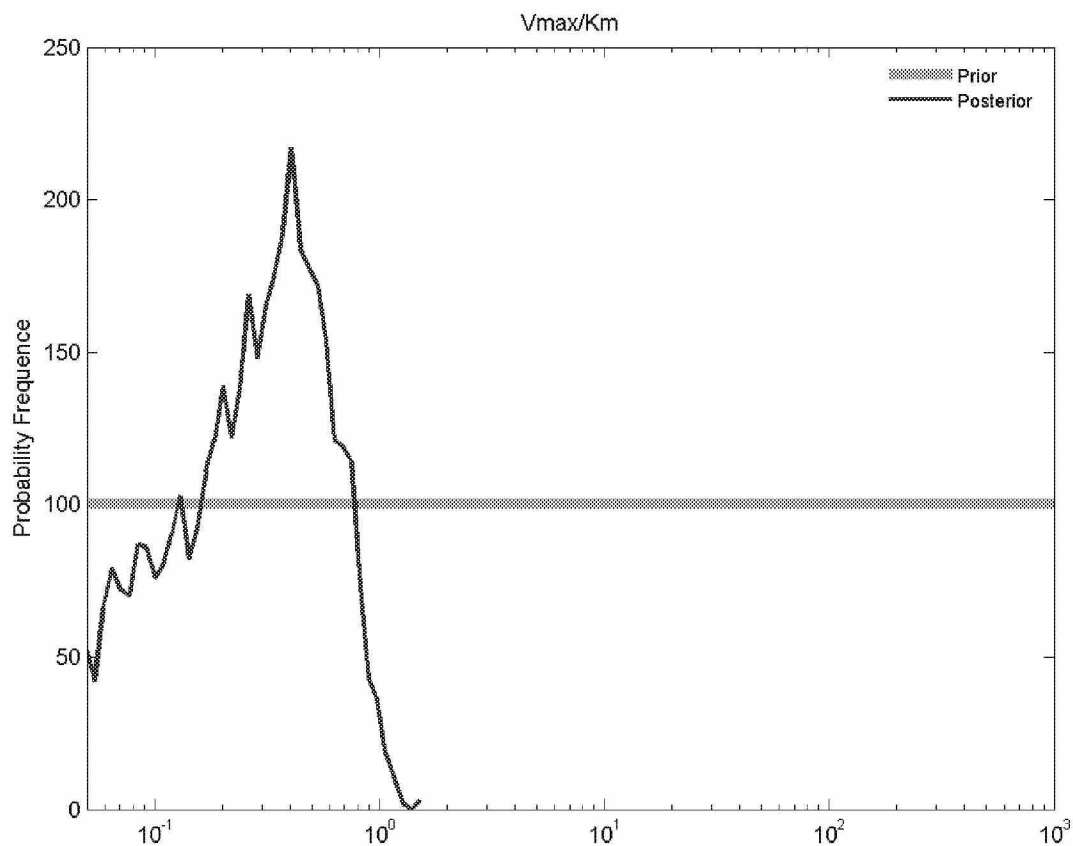
Note: Chloroprene headspace concentrations (symbols) and model simulations (lines) based on parameter values reported in Table 4.

Figure 16  
Representative comparison of uniform prior and posterior distributions for human (pooled mixed gender) liver microsomal  
metabolism parameters



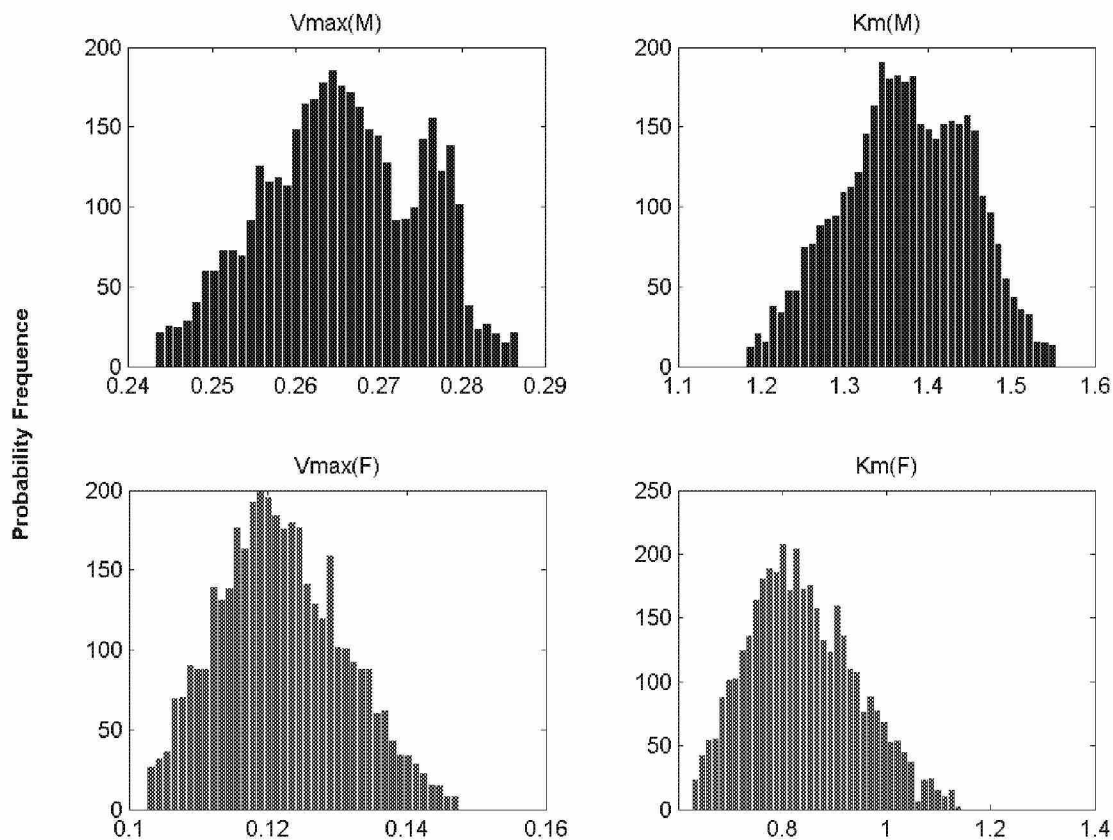
Note: Vmax ( $\mu\text{mol/hr/mg}$  microsomal protein) or Km ( $\mu\text{mol/L}$ ) posterior frequency counts (per 4000 simulations).

Figure 17  
Representative comparison of uniform prior and posterior distributions for oxidative metabolism  
of chloroprene in human (pooled mixed gender) lung microsomes



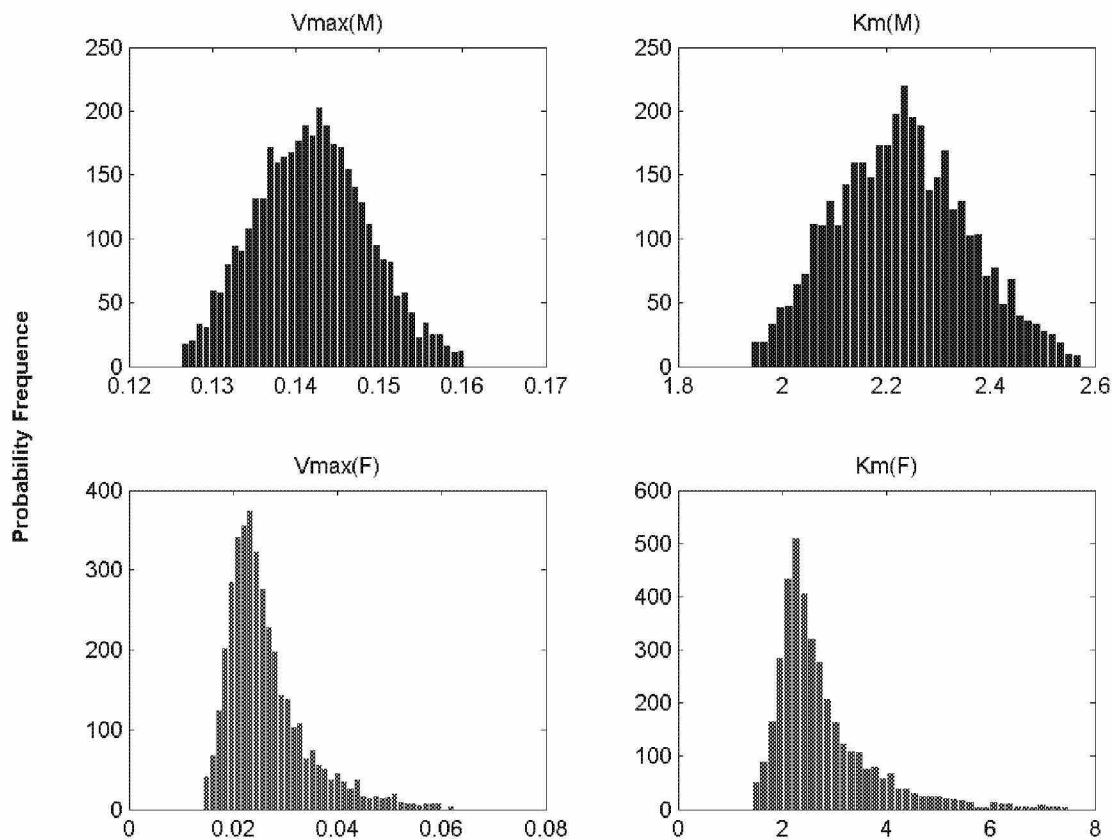
Note:  $V_{max}/K_m$  (L/hr/g microsomal protein) posterior frequency counts (per 4000 simulations).

Figure 18  
Probability frequency of chloroprene oxidative metabolism parameters in male (M) and female (F) B6C3F1 mouse liver microsomes



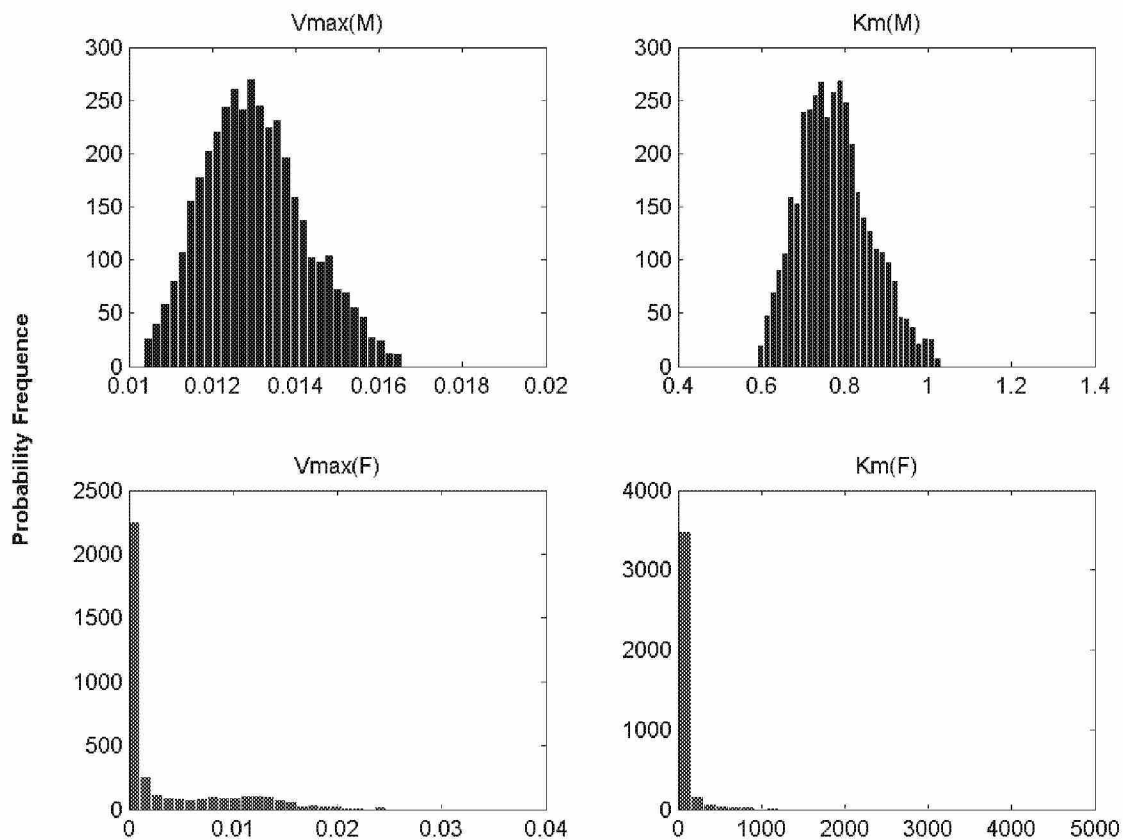
Note: Vmax ( $\mu\text{mol/hr/mg}$  microsomal protein) or Km ( $\mu\text{mol/L}$ ) posterior frequency counts (per 4000 simulations).

Figure 19  
Probability frequency of chloroprene oxidative metabolism parameters in male (M) and female (F) B6C3F1 mouse lung microsomes



Note: Vmax ( $\mu\text{mol/hr/mg}$  microsomal protein) or Km ( $\mu\text{mol/L}$ ) posterior frequency counts (per 4000 simulations).

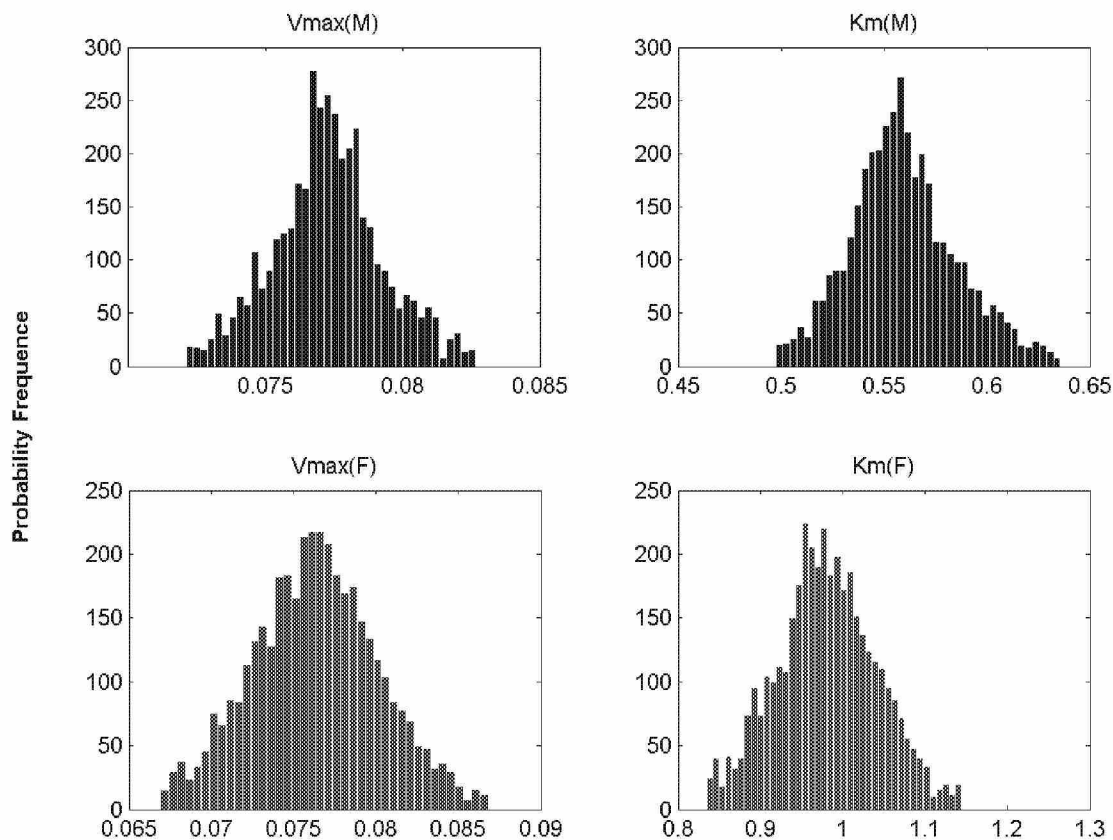
Figure 20  
Probability frequency of chloroprene oxidative metabolism parameters in male (M) and female (F) B6C3F1 mouse kidney microsomes



Note: Vmax ( $\mu\text{mol/hr/mg}$  microsomal protein) or Km ( $\mu\text{mol/L}$ ) posterior frequency counts (per 4000 simulations).

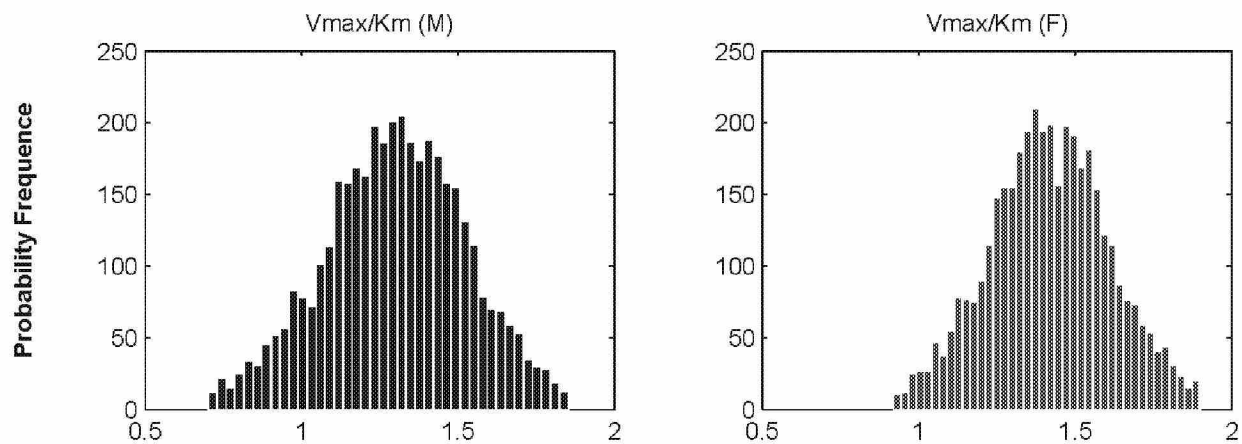


Figure 21  
Probability frequency of chloroprene oxidative metabolism parameters in male (M) and female (F) Fischer rat liver microsomes



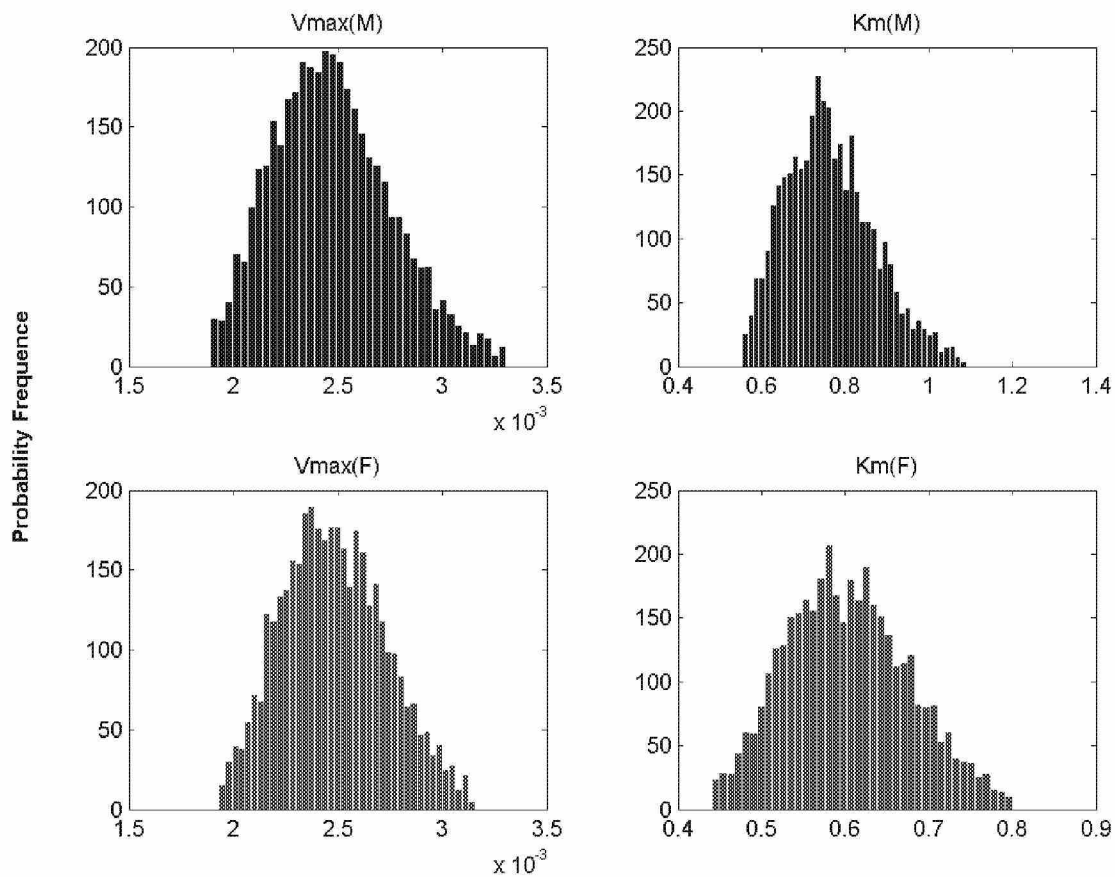
Note: Vmax ( $\mu\text{mol/hr/mg}$  microsomal protein) or Km ( $\mu\text{mol/L}$ ) posterior frequency counts (per 4000 simulations).

Figure 22  
Probability frequency of chloroprene oxidative metabolism parameters in male (M) and female (F) Fischer rat lung microsomes



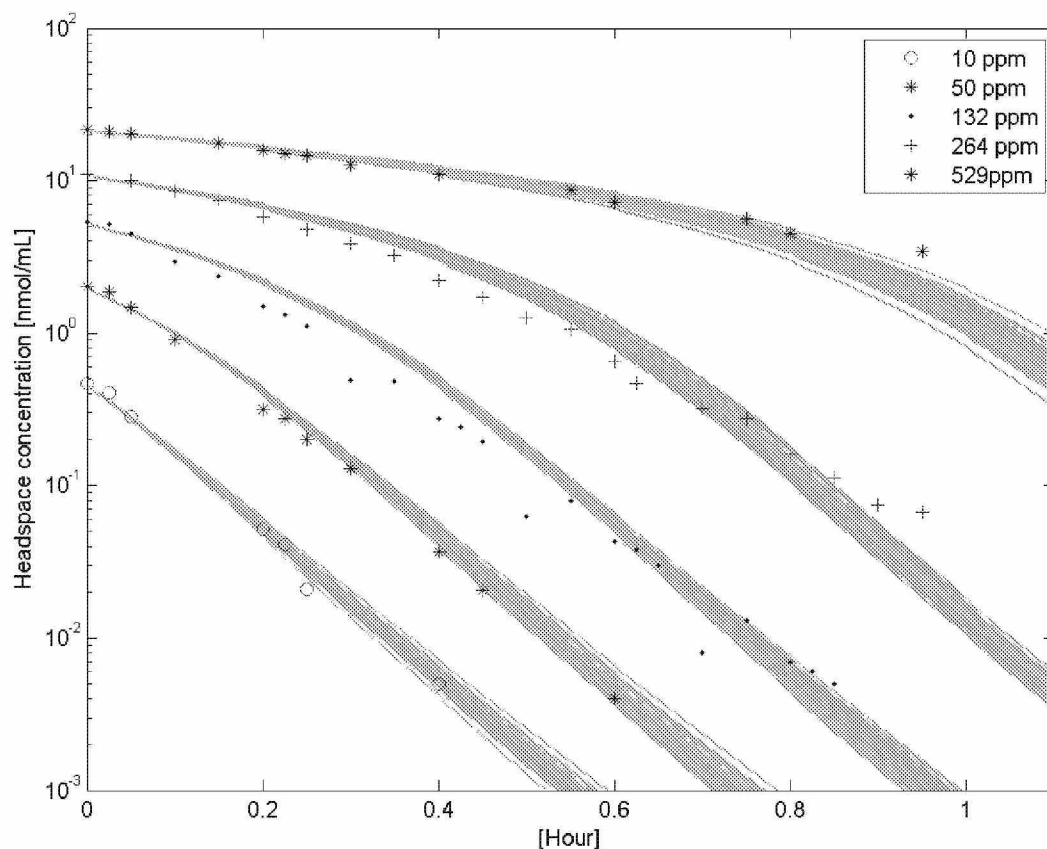
Note: Vmax/Km (L/hr/g microsomal protein) posterior frequency counts (per 4000 simulations).

Figure 23  
Probability frequency of chloroprene oxidative metabolism parameters in male (M) and female (F) Fischer rat kidney microsomes



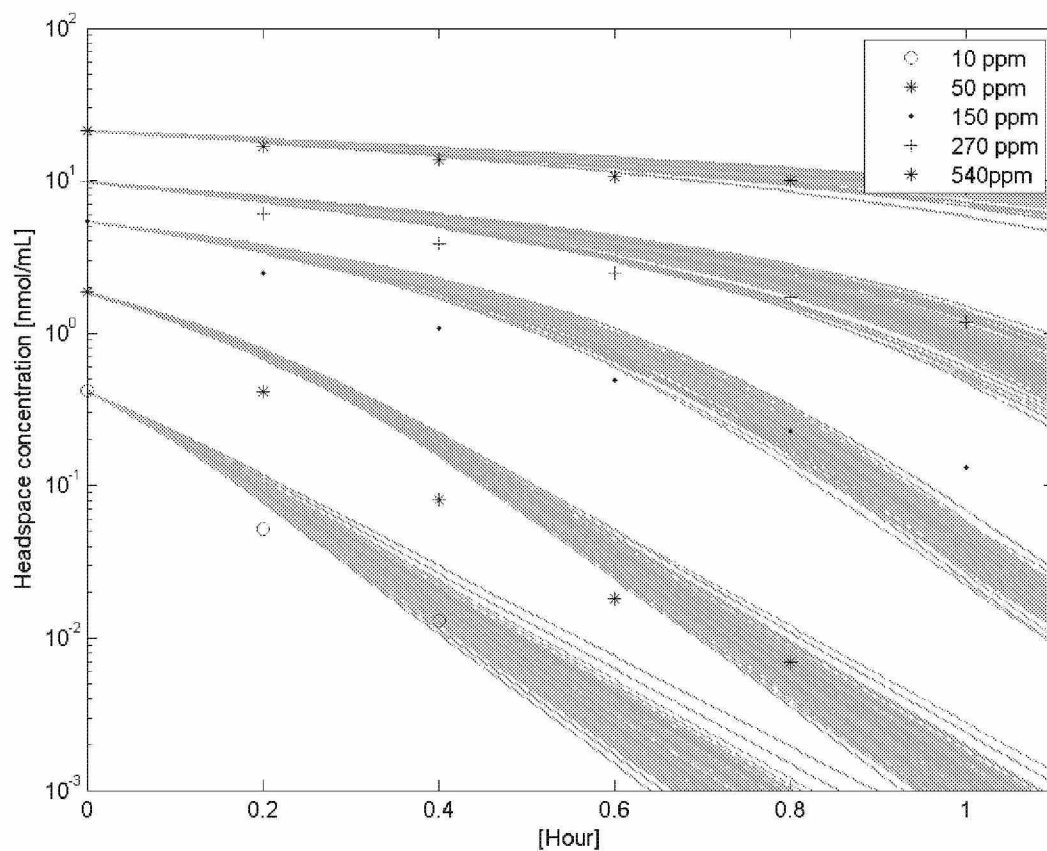
Note: Vmax ( $\mu\text{mol/hr/mg}$  microsomal protein) or Km ( $\mu\text{mol/L}$ ) posterior frequency counts (per 4000 simulations).

Figure 24  
Distribution of chloroprene oxidative metabolism time course in male B6C3F1 mouse liver  
microsomes



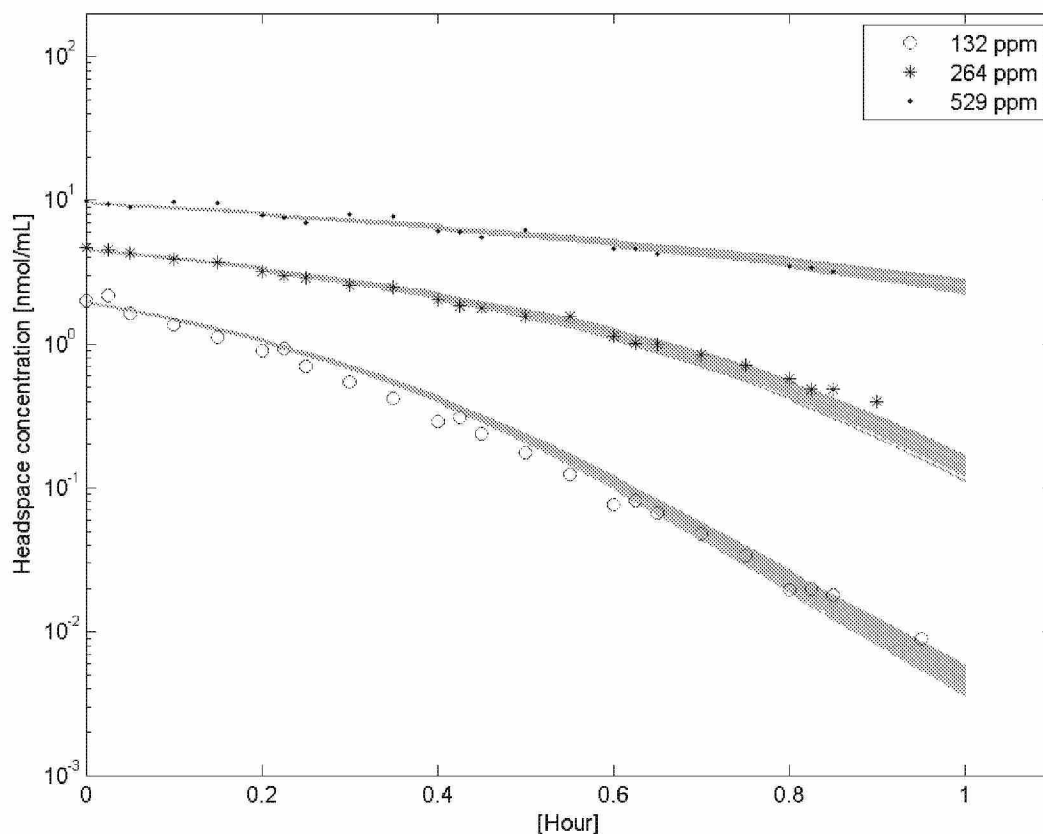
Note: Chloroprene headspace concentrations (symbols) and model simulations (50 lines) based on posterior distribution for parameter values as reported in Table 5. Simulations for each starting concentration represent 50 sets of model parameters randomly drawn from the posterior distributions.

Figure 25  
Distribution of chloroprene oxidative metabolism time course in female B6C3F1 mouse liver  
microsomes



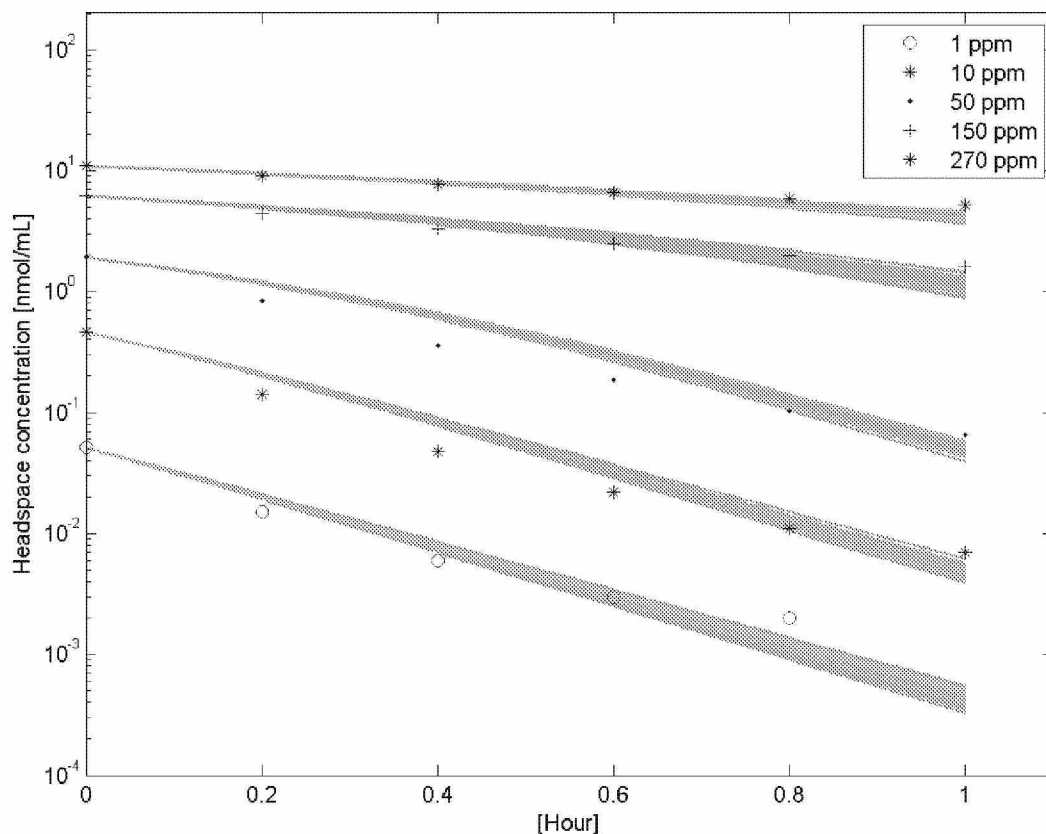
Note: Chloroprene headspace concentrations (symbols) and model simulations (50 lines) based on posterior distribution for parameter values as reported in Table 5. Simulations for each starting concentration represent 50 sets of model parameters randomly drawn from the posterior distributions.

Figure 26  
Distribution of chloroprene oxidative metabolism time course in male Fischer rat liver  
microsomes



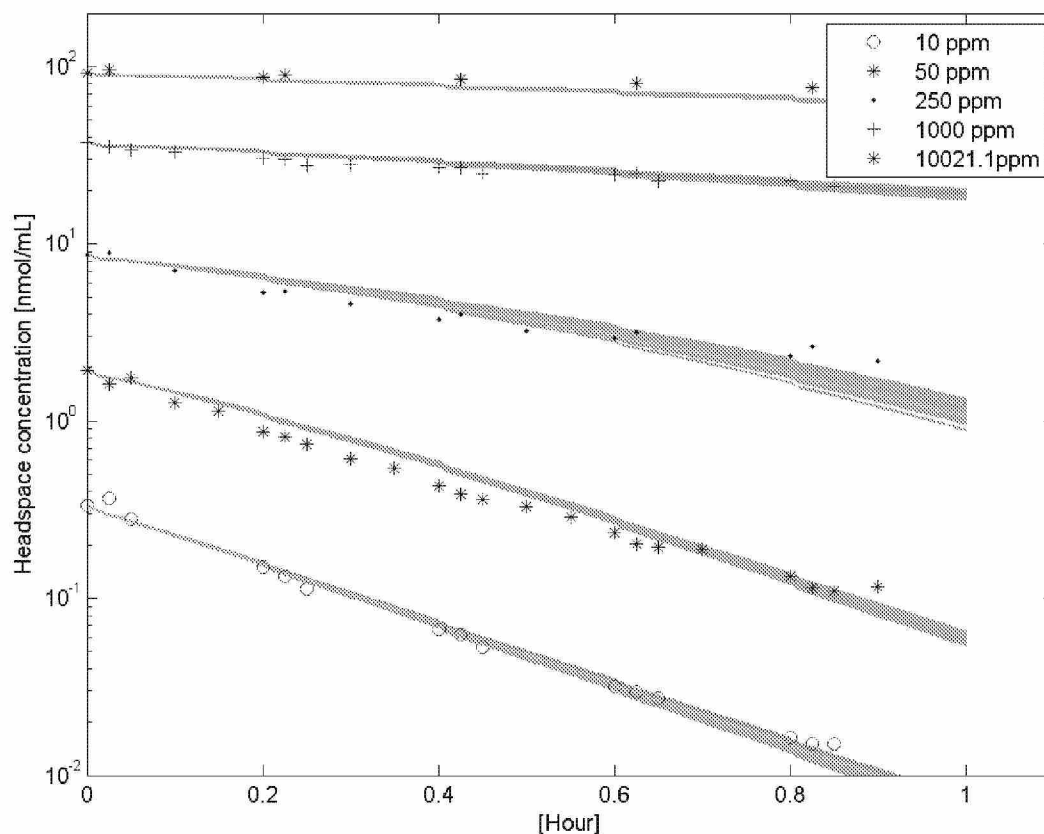
Note: Chloroprene headspace concentrations (symbols) and model simulations (50 lines) based on posterior distribution for parameter values as reported in Table 5. Simulations for each starting concentration represent 50 sets of model parameters randomly drawn from the posterior distributions.

Figure 27  
Distribution of chloroprene oxidative metabolism time course in female Fischer rat liver  
microsomes



Note: Chloroprene headspace concentrations (symbols) and model simulations (50 lines) based on posterior distribution for parameter values as reported in Table 5. Simulations for each starting concentration represent 50 sets of model parameters randomly drawn from the posterior distributions.

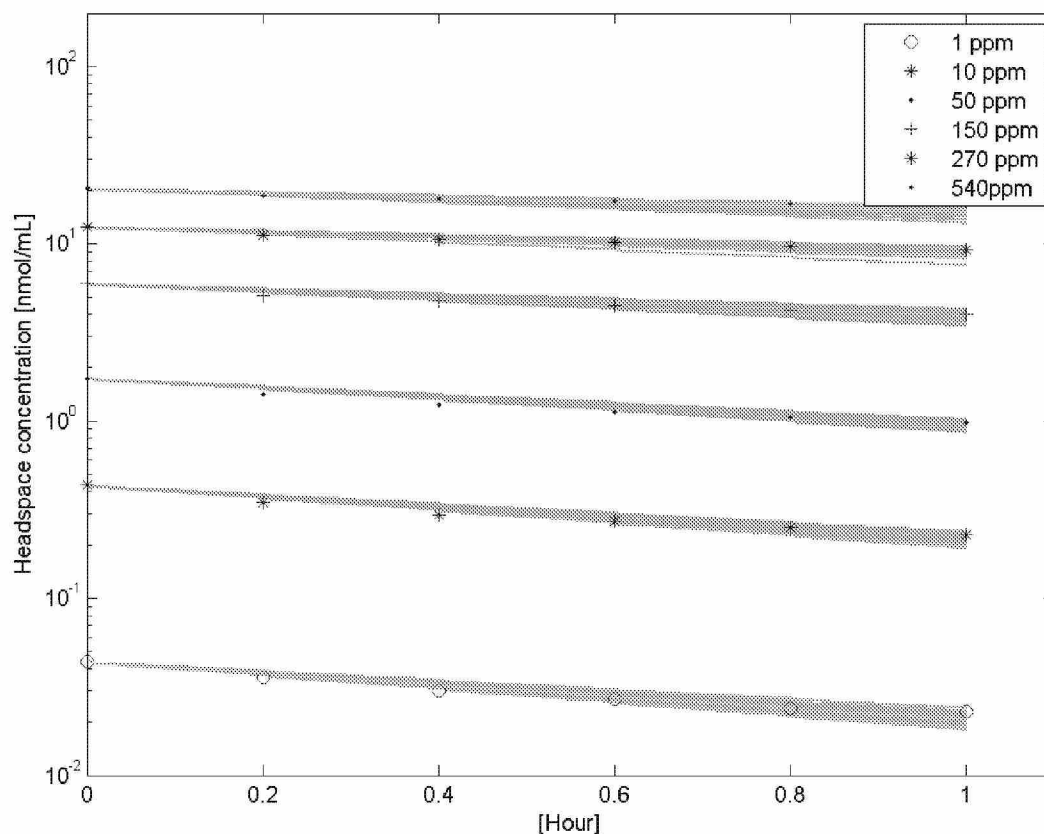
Figure 28  
Distribution of chloroprene oxidative metabolism time course in male B6C3F1 mouse lung  
microsomes



Note: Chloroprene headspace concentrations (symbols) and model simulations (50 lines) based on posterior distribution for parameter values as reported in Table 5. Simulations for each starting concentration represent 50 sets of model parameters randomly drawn from the posterior distributions.

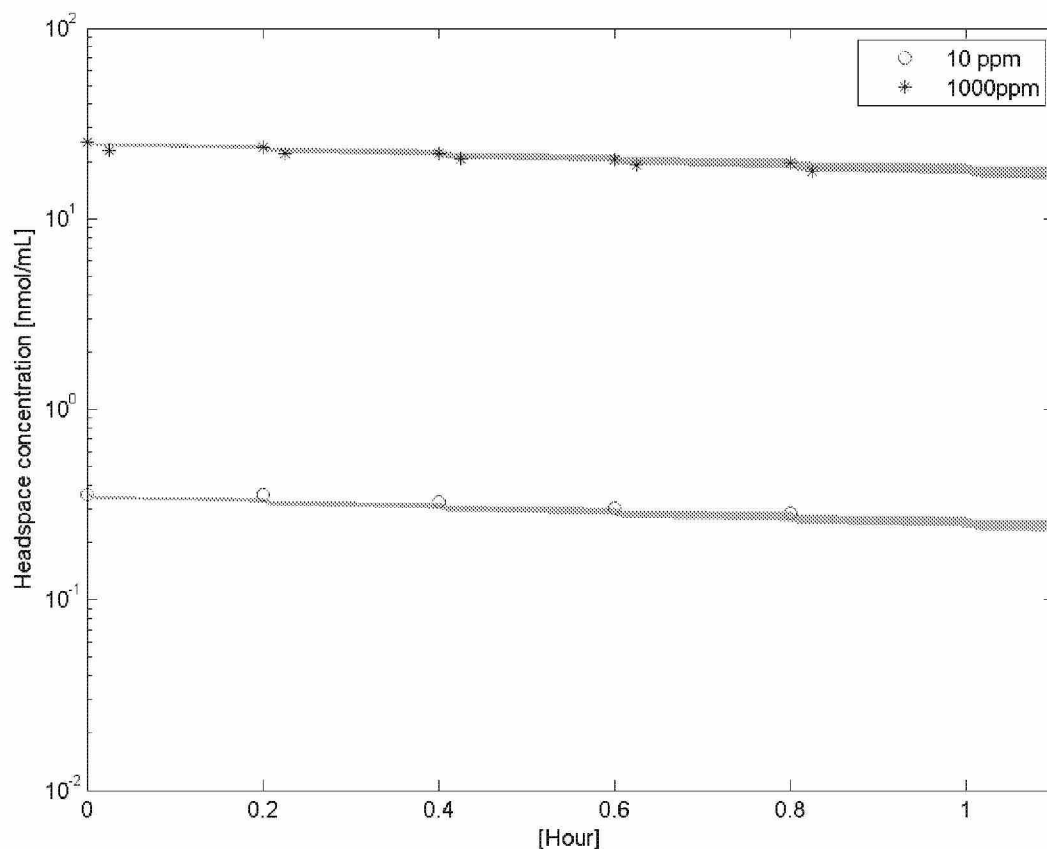


Figure 29  
Distribution of chloroprene oxidative metabolism time course in female B6C3F1 mouse lung  
microsomes



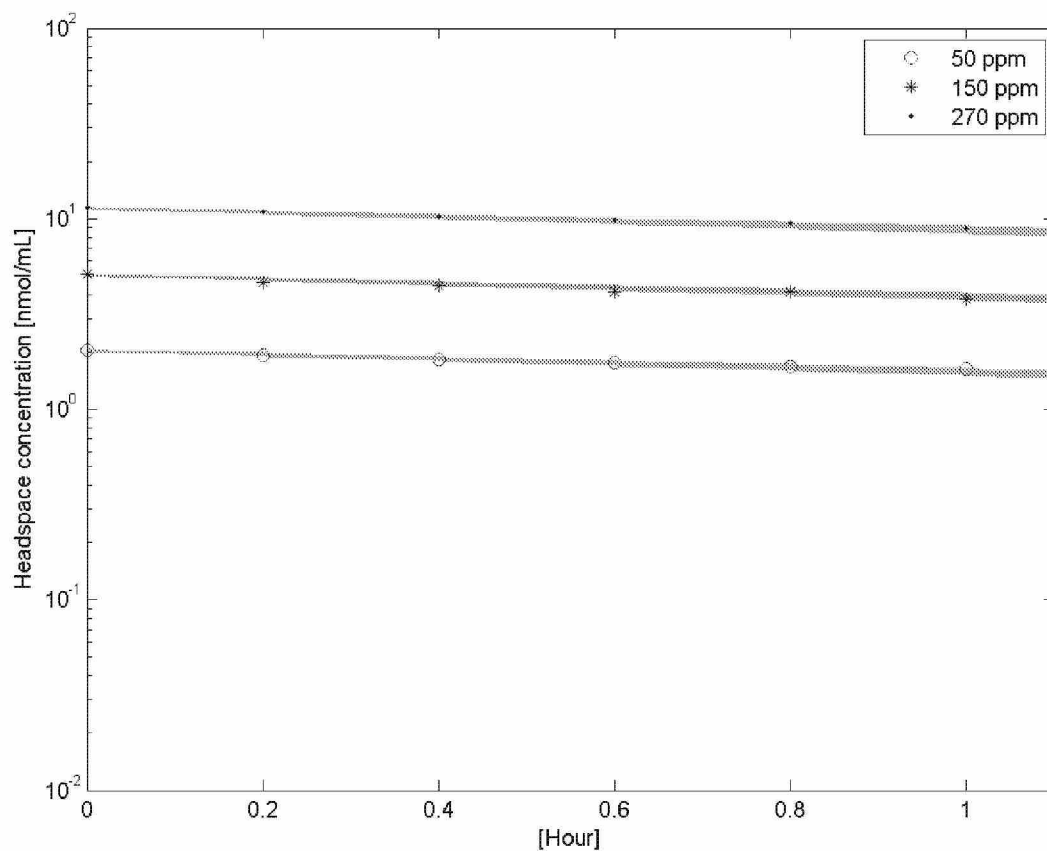
Note: Chloroprene headspace concentrations (symbols) and model simulations (50 lines) based on posterior distribution for parameter values as reported in Table 5. Simulations for each starting concentration represent 50 sets of model parameters randomly drawn from the posterior distributions.

Figure 30  
Distribution of chloroprene oxidative metabolism time course in male Fischer rat lung  
microsomes



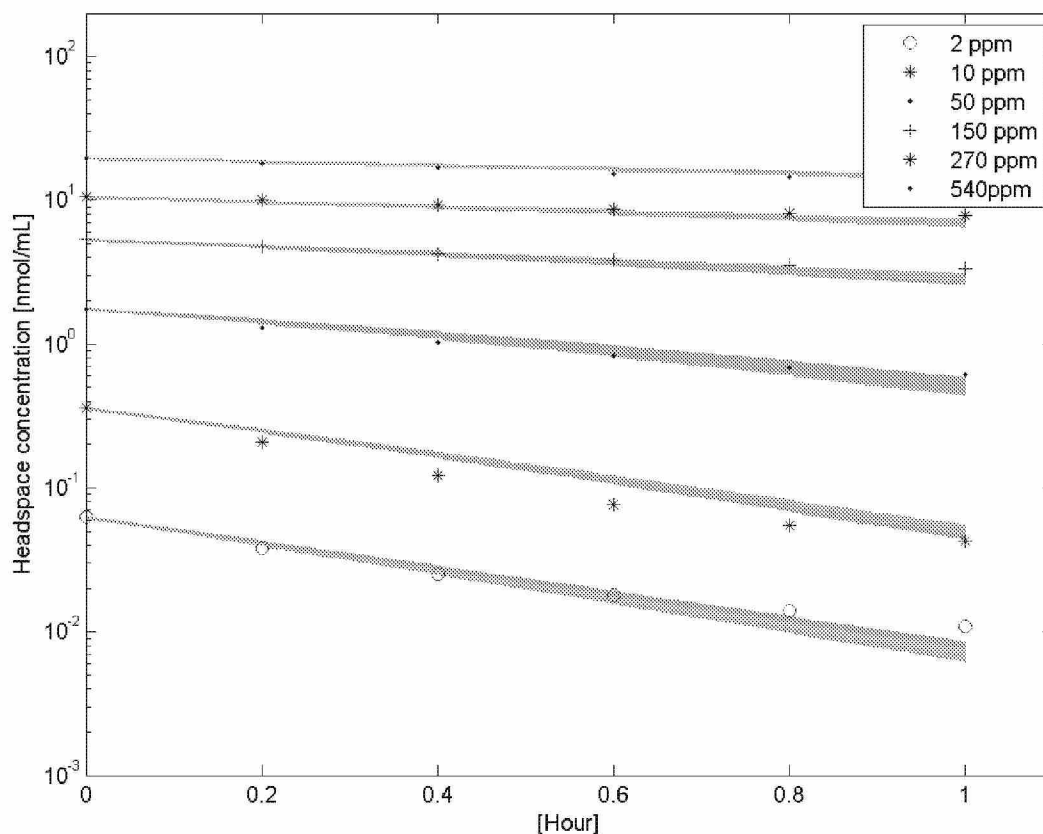
Note: Chloroprene headspace concentrations (symbols) and model simulations (50 lines) based on posterior distribution for parameter values as reported in Table 5. Simulations for each starting concentration represent 50 sets of model parameters randomly drawn from the posterior distributions.

Figure 31  
Distribution of chloroprene oxidative metabolism time course in female Fischer rat lung  
microsomes



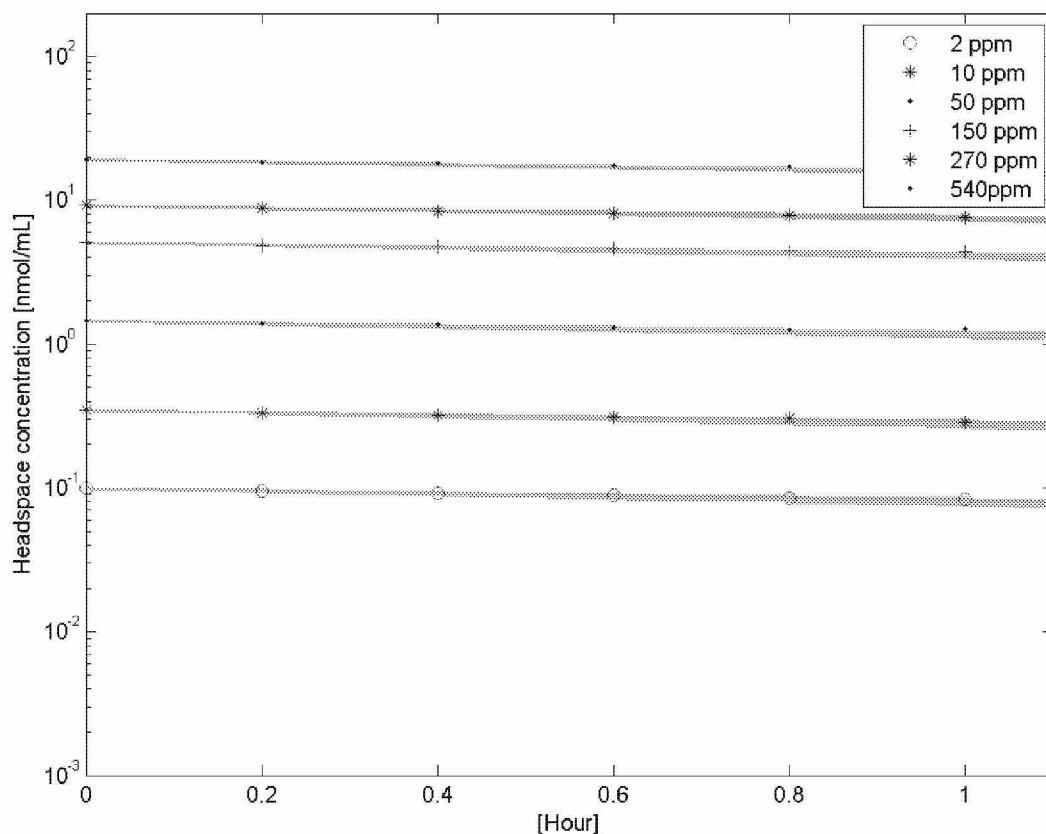
Note: Chloroprene headspace concentrations (symbols) and model simulations (50 lines) based on posterior distribution for parameter values as reported in Table 5. Simulations for each starting concentration represent 50 sets of model parameters randomly drawn from the posterior distributions.

Figure 32  
Distribution of chloroprene oxidative metabolism time course in male B6C3F1 mouse kidney  
microsomes



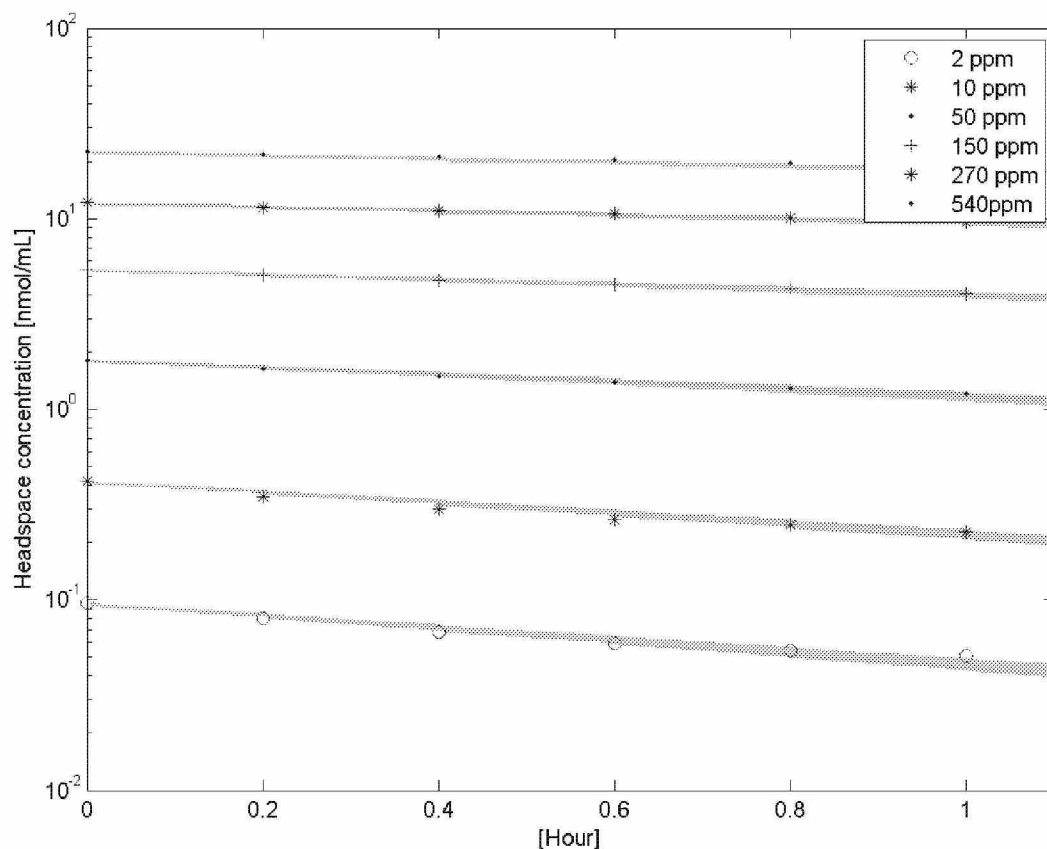
Note: Chloroprene headspace concentrations (symbols) and model simulations (50 lines) based on posterior distribution for parameter values as reported in Table 5. Simulations for each starting concentration represent 50 sets of model parameters randomly drawn from the posterior distributions.

Figure 33  
Distribution of chloroprene oxidative metabolism time course in female B6C3F1 mouse kidney  
microsomes



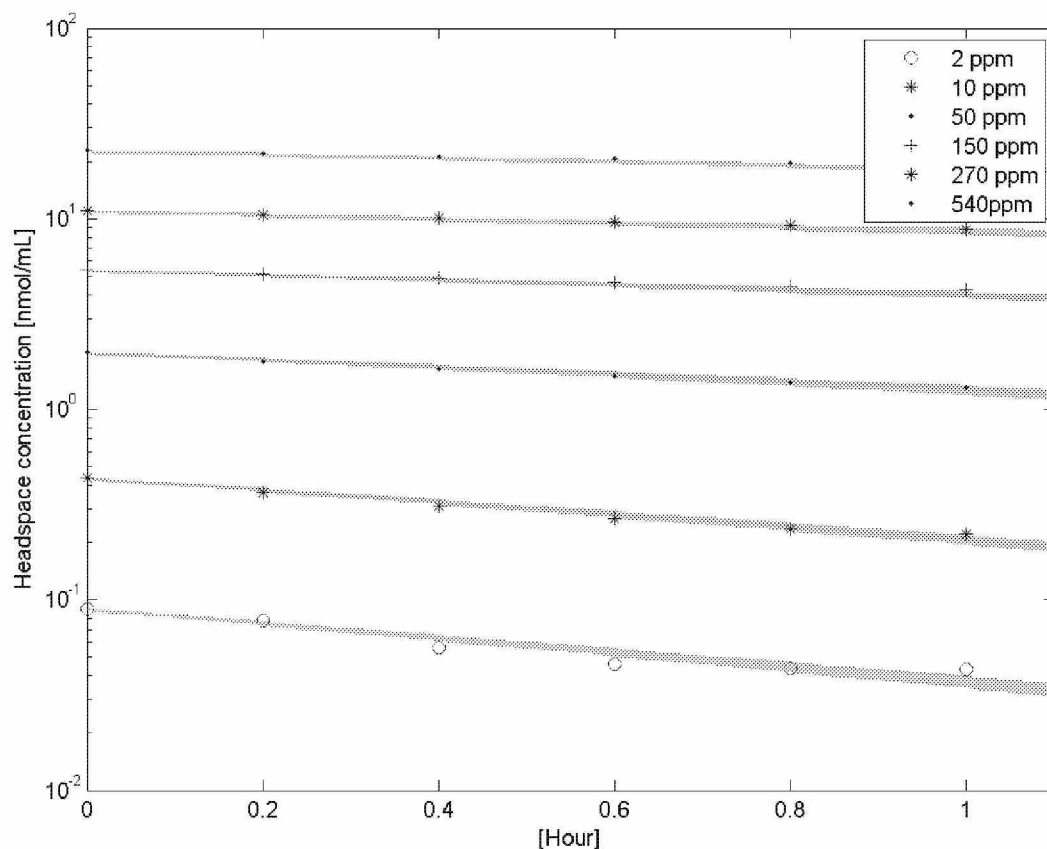
Note: Chloroprene headspace concentrations (symbols) and model simulations (50 lines) based on posterior distribution for parameter values as reported in Table 5. Simulations for each starting concentration represent 50 sets of model parameters randomly drawn from the posterior distributions.

Figure 34  
Distribution of chloroprene oxidative metabolism time course in male Fischer rat kidney  
microsomes



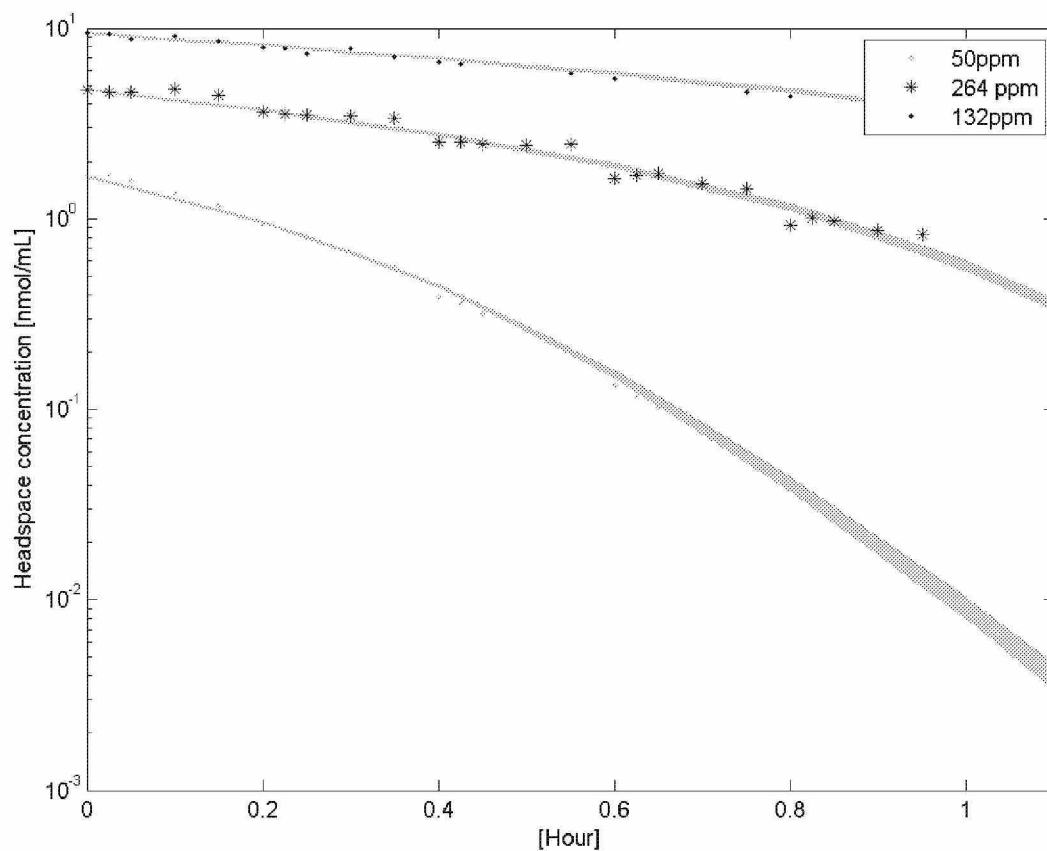
Note: Chloroprene headspace concentrations (symbols) and model simulations (50 lines) based on posterior distribution for parameter values as reported in Table 5. Simulations for each starting concentration represent 50 sets of model parameters randomly drawn from the posterior distributions.

Figure 35  
Distribution of chloroprene oxidative metabolism time course in male Fischer rat kidney  
microsomes



Note: Chloroprene headspace concentrations (symbols) and model simulations (50 lines) based on posterior distribution for parameter values as reported in Table 5. Simulations for each starting concentration represent 50 sets of model parameters randomly drawn from the posterior distributions.

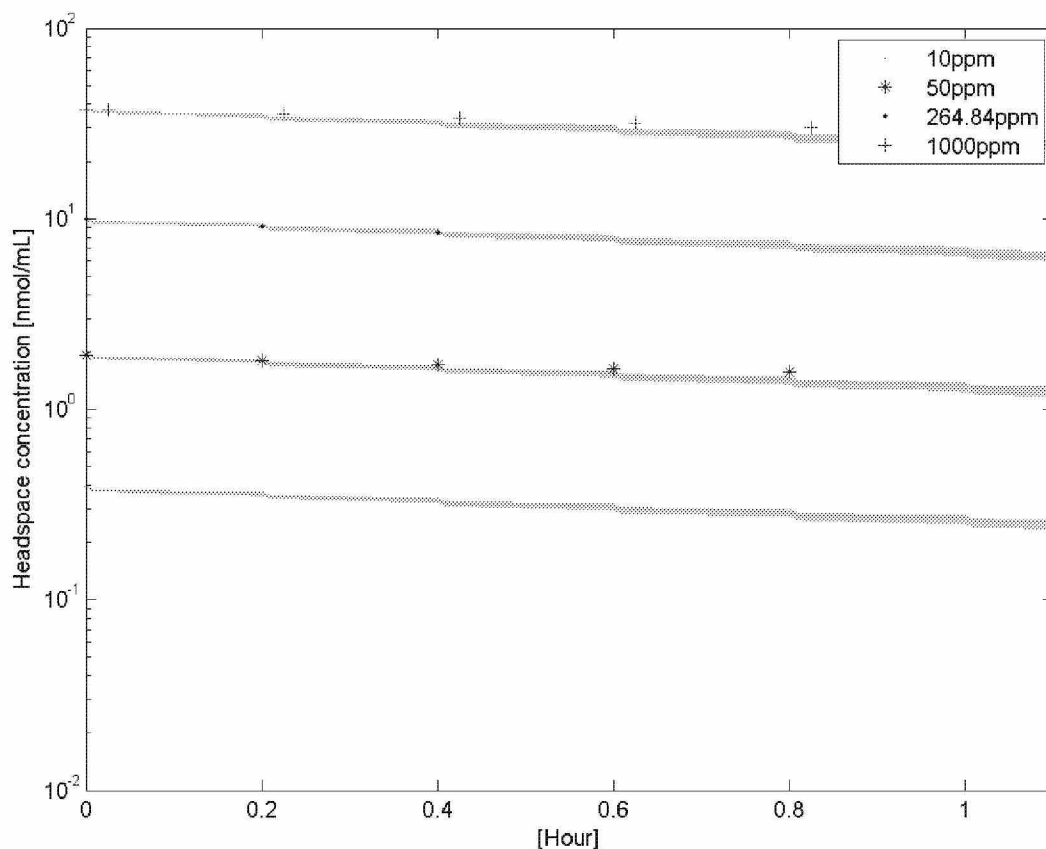
Figure 36  
Distribution of chloroprene oxidative metabolism time course in human (pooled mixed gender)  
liver microsomes



Note: Chloroprene headspace concentrations (symbols) and model simulations (50 lines) based on posterior distribution for parameter values as reported in Table 5. Simulations for each starting concentration represent 50 sets of model parameters randomly drawn from the posterior distributions.



Figure 37  
Distribution of chloroprene oxidative metabolism time course in human (pooled mixed gender)  
lung microsomes



Note: Chloroprene headspace concentrations (symbols) and model simulations (50 lines) based on posterior distribution for parameter values as reported in Table 5. Simulations for each starting concentration represent 50 sets of model parameters randomly drawn from the posterior distributions.

## APPENDICES

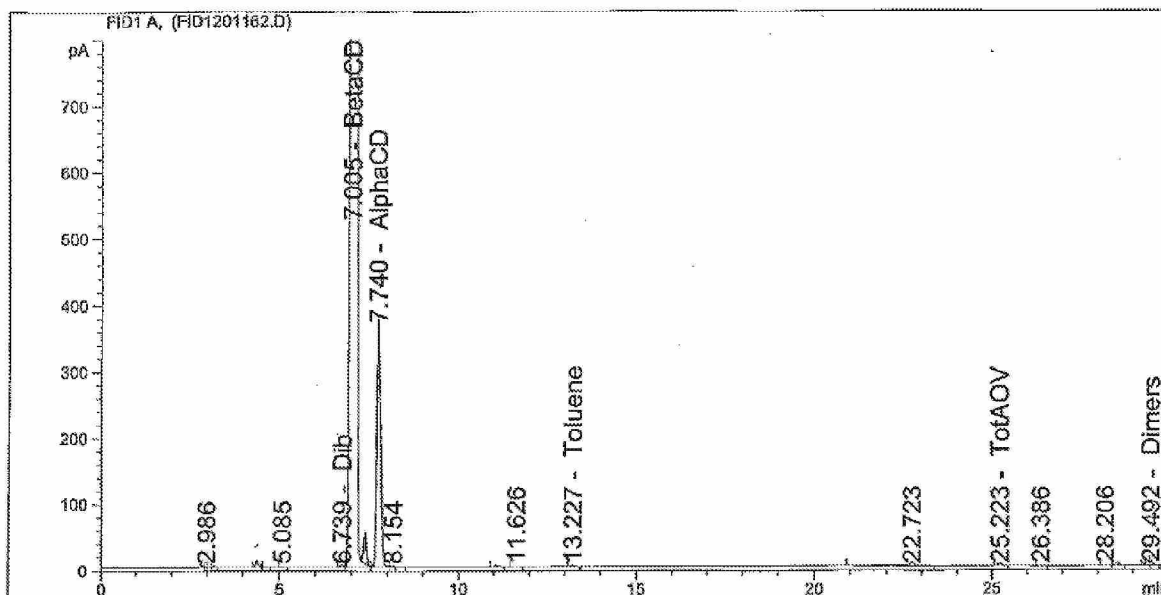
**Appendix A**  
**Purity Analysis of  $\beta$ -Chloroprene Provided by the Sponsor's Supplier**

Data File C:\CHEM32\2\DATA\FID1: 2...  
Sample Name: PW0902050006

```
=====
Acq. Operator   : BELLTA2
Acq. Instrument : Instrument 2
Injection Date  : 05-Feb-09, 10:23:45
Location       : Vial 101
Inj            : 1
Inj Volume     : 1 µl

Method          : C:\CHEM32\2\METHODS\1223_FT.M
Last changed    : 2/22/2008 7:17:17 AM by FISKSD
Method Info     : Adopted from Diamines 1223 Method:
                   CRUDE CD TO STORAGE - CA,CB
                   CRUDE CD FROM COND - CC,CD
                   CD REACTOR EFFLUENT - CQ
                   CRUDE CD 1373 TK - LA
                   RECYCLE CD - #1TK-LB, #2TK-LC
                   CD REFINER MAKE - LG
                   REFINED CD TO SMU - LH
=====
```

Sample Info : LH



Normalized Percent Report

```
=====
Sorted By      : Signal
Calib. Data Modified : 2/7/2008 2:55:13 PM
Multiplier     : 1.0000
Dilution       : 1.0000
Sample Amount   : 1.00000 (Wt %) (not used in calc.)
Do not use Multiplier & Dilution Factor with ISTDs
=====
```

Data File C:\CHEM32\2\DATA\FID1201162.D  
Sample Name: PW0902050006

Signal 1: FID1 A,

RetTime [min]	Type	Area [pA*s]	Amt/Area	Norm %	Grp	Name
3.070	VV	2.59367	2.26491e-5	0.000023	1	MVA+BT
6.739	BV	20.08306	7.40682e-7	5.91327e-6	1	Dib
7.005	VB S+	3.70246e5	6.73627e-4	99.146237	2	BetaCD
7.364	BV T	278.51874	4.37484e-6	0.000484		1ChlBut2
7.740	VV T	2807.87915	7.12311e-4	0.795086	2	AlphaCD
10.796		-	-	-	3	2CPA
11.070	BB	19.48002	2.23001e-4	0.001727	3	3CPA
12.119		-	-	-		Meso
12.546		-	-	-	3	1CPA
13.227	BB	10.39957	1.21217e-4	0.000501		Toluene
13.698		-	-	-	4	DCbutanes
13.943		-	-	-		34DCB
14.449		-	-	-		Cellosolve
15.760		-	-	-		4VCH
16.701		-	-	-		Cis14DCB
18.000		-	-	-		Trans14DCB
25.223	BB	33.66175	7.50607e-5	0.001004		TotAOV
28.547	BB	31.02670	5.52082e-4	0.006809	5	Dimers
29.389	BV +	50.80355	1.05035e-3	0.021213		CDimers
29.492	VB	37.12034	1.82046e-3	0.026863	5	Dimers

Totals : 100.000000

Group summary :

Group ID	Use	Area [pA*s]	Norm. %	Group Name
1		22.67672	2.92657e-5	TotLB
2		3.73054e5	99.941322	TotCD
3		19.48002	1.72688e-3	CPAS
4		0.00000	0.000000	DCBanes
5		68.14704	3.36725e-2	TotDimers

3 Warnings or Errors :

Warning : Calibration warnings (see calibration table listing)  
Warning : Time reference compound(s) not found  
Warning : Elution order of calibrated compounds may have changed

\*\*\* End of Report \*\*\*

**Appendix B**  
**Human Kidney Microsome Data Sheet**